

Magnetotelluric evidence for trapped fluids beneath the seismogenic zone of the Mw6.0 Anjar earthquake, Kachchh intraplate region, northwest India

^{1,3}Mehul Nagar, ^{1,2}Pavan Kumar, G*, ^{1,4}Mahesh, P., ¹Rakesh, N, ¹Avinash Kumar Chouhan, ²Nagarujna, D. ¹Sumer Chopra and ^{2,1}M. Ravi Kumar

¹Institute of Seismological Research, Raisan, Gandhinagar – 382 009

²CSIR-National Geophysical Research Institute (CSIR-NGRI),
Uppal Road, Habsiguda, Hyderabad - 500 007

³ Department of Earth Sciences, Gujarat University, Ahmedabad

⁴ CSIR-National institute of Oceanography (CSIR-NIO), Dona Paula, Goa-403004

Corresponding author: pavan.ngri@gmail.com

G. Pavan Kumar

Scientist, Electromagnetic Geophysics Group

CSIR-National Geophysical Research Institute (CSIR-NGRI),

Uppal Road, Habsiguda, Hyderabad - 500 007

Contact No.: +91-9574012249

Abstract

Lithospheric rheological heterogeneities across a rift play a significant role in intraplate deformation and seismic activity. The Kachchh rift in the northwestern part of the India has not only experienced lithospheric stretching but also witnessed large magnitude devastating earthquakes. Here, we present the results of a magnetotelluric (MT) investigation carried out in the southeastern part of the Kachchh intraplate region illuminating the seismogenic zone of the 1956 Anjar earthquake (Mw 6.0). The two-dimensional geoelectrical model derived from the MT data acquired at 21 sites along a NE-SW profile reveals assemblage of conductive and resistive zones in the upper and the mid crustal depths in the close vicinity of the major fault zones and the hypocentral depths. The results reveal a very high conductive zone near the Moho, affirming the presence of an upper mantle fluidized zone. Unlike the South Wagad Fault, the Kachchh mainland fault and the Katrol Hill Fault do not have a downward lower crustal extension, and terminate at the mid crustal depths. We suggest that the presence of trapped fluids in the brittle-ductile transition zone (12-15km) and their seepage to the resistive plutons might be a possible mechanism for triggering the 1956 event as well as the current seismic activity in the region.

Key words: Magnetotellurics, Anjar earthquake, intraplate seismicity, fluids, trapped magma

Key Points:

Evidence for trapped fluids in the seismically active Kachchh intraplate region

High level of upper crustal heterogeneity beneath the epicentral region of the Anjar earthquake

A plausible model for genesis of large magnitude earthquakes in the Kachchh region

Introduction:

The Deccan Volcanic Province (DVP), located in the western part of the Indian subcontinent evolved at the Cretaceous-Tertiary transition, as a consequence of torching of the Indian plate by a mantle plume at the Reunion hotspot (Morgan, 1981; Cox, 1983; Watts & Cox, 1989). During 69-65 Ma, the region has experienced massive volcanic eruptions in a short period of less than 1 Myr (Duncan & Pyle, 1988), now manifested as one of the largest continental flood basalt provinces in the world. Geochemical studies suggest that the volcanism is related to partial melting of a massive mantle plume originating in the vicinity of the core-mantle boundary (Campbell & Griffiths, 1990). Due to its dynamic history, tectonics and complex geological evolution, the region has evoked a lot of scientific interest since many decades. The Kachchh rift basin (KRB) located in the northwestern DVP (Fig.1) is an east-west oriented palaeo-rift basin with syn-rift sedimentation that continued through the Jurassic up to the Early Cretaceous, as the Indian plate separated from Africa and drifted northward. The collision between the Indian and the Eurasian plates during the middle to late Tertiary time not only gave rise to the Himalayan mountain belt but also lead to the rift termination and initiation of basin inversion during the end of Tertiary (Biswas, 1987, 2005), due to the onset of a compressive stress regime produced by the plate collision. Due to the Mesozoic rifting episodes, the crust in the region is highly extended. It has been suggested that the Mesozoic sedimentation took place during the post-rift period and then undergone a compressive inversion resulting in the present structural frame work.

Since historical past, the Kachchh region has been experiencing significant number of large to moderate sized earthquakes (Fig. 1b). These include the 1819 Kachchh (Allahbund) earthquake (M 7.8), 1845 Lakhpat earthquake (Mw6.3), 1956 Anjar earthquake (Mw6.0) and the deadliest 2001 Bhuj earthquake (Mw7.7) (Fig. 1), making it one of the most seismically active intraplate regions of the world. The seismic activity is still continuing, as seen from the earthquake distribution during 2007-2017 (figure 2). Since the 1819 earthquake occurred during the non-instrumental period, its exact source parameters are not well known. It is believed that the earthquake had produced significant ground deformation that caused folding of regions near coastal regions, formation of 80-km-long natural dam (the Allah Bund or Dam of God) across the Kori (Korree) branch of the Indus river, widespread liquefaction and a local tsunami (Bilham, 1999). Dislocation models based on the deformation data and subsequent geological models reveal a 50-70°N dipping fault plane, along which a dip-slip type of motion occurred (Bilham, 1999). There are not enough seismological and geophysical constraints to infer the precise location of the epicentre, type of faulting and the geometry of the fault plane. Recently, Pavan Kumar et al. (2019) have carried out electromagnetic investigations in the western part of the Great Rann of Kachchh and delineated an upper crustal south dipping conductor, interpreted as a subsurface image of the Allah-bund Fault (ABF) or its splay. The

seismological aspects of the 1956 Anjar earthquake have been elaborately discussed by Chung and Gao (1995). The Anjar earthquake occurred on July 21, 1956 ($M_w = 6.0$) with a maximum intensity of IX, which caused considerable damage and casualties in the Kachchh region. Teleseismic waveform analysis (Chung and Gao, 1995) revealed a reverse faulting mechanism (strike = 235° , dip = 46.5° , rake = 85°) with a high stress drop value of 162 bar. Choudhury et al. (2017) estimated the strong ground motions due to the Anjar earthquake at 12 sites using the empirical Green's function approach. Their study predicted a Peak Ground Acceleration (PGA) of 250 to 300 gals in the epicentral region. The isoseismal pattern strongly suggests a very low attenuation factor (Q_s) for the Kachchh-Cambay graben (Johnston, 1996). The model supports the idea of Jin & Aki (1988) that large intraplate earthquakes occur preferentially within low-Q (high seismic wave attenuation) regions. Further, the depth migrated seismic reflection studies carried out by Sarkar et al. (2007) along three profiles in the eastern part of the Kachchh region, estimated the Moho depth in the range of 35 (at the coast) to 45km (near the 2001 Bhuj epicentral zone), suggesting a gentle dip from south to the north. In addition to strong reflectivity at the crust-mantle boundary, a couple of prominent sub-Moho reflectivity zones are identified, which they interpreted as igneous intrusions and fluidized zones emplaced during the rift formation. Further, a blind basement fault, nearly coinciding with the geologically known Katrol Hill fault, inferred ~ 10 km north of the Anjar town, was associated with the 1956 earthquake (Sarkar et al. 2007).

A number of geophysical studies have been carried out to understand the mechanisms responsible for the 2001 Bhuj earthquake and its continued aftershock activity (Kayal et al., 2002; Mandal and Pujol, 2006; Chandrasekhar et al., 2009; Naganjaneyulu et al., 2010; Chandrasekhar et al. 2012; Rao et al., 2015; Pavan Kumar et al., 2017a, & b). Plate tectonic theory explains the occurrence of earthquakes at discrete plate boundaries. Intraplate earthquakes occur in an otherwise stable crust located far away from any plate boundary, and more destructive. The occurrence of these earthquakes cannot be explained by classical plate tectonics, and as such, are a topic of great scientific debate (Mooney and White, 2010). The KRB being far (~ 400 km) from the plate boundary, the deformation mechanism and the seismicity cannot be explained using the traditional theory of the plate tectonics. In general, it has been proposed that the lithospheric rheological heterogeneities across a rift play a significant role in intraplate earthquake genesis and the stresses developed at plate boundaries are transferred over long distances affecting the causative deformation processes (Calignano et al., 2015; Yin et al., 2017). A magnetotelluric (MT) study by Chandrashekar et al. (2012) in the eastern part of the Kachchh region inferred a basal detachment, marking a transition zone between the crust and the upper mantle, intersected by a reverse fault. Pavan Kumar et al. (2017) have carried out MT studies along two N-S profiles in the seismically active eastern part of the Kachchh region (Fig. 1a). The study

reveals presence of a sub-moho fluid reservoir below the epicentre of the 2001 Bhuj earthquake (Mw 7.7). They suggested that the mantle reaching South Wagad and the north Wagad Faults serve as feeders for the fluid flow from the reservoir to the epicentral depths. The authors postulated that the migration of fluids from the reservoir and their injection into the fractured regions of the crust explains the aftershock activity in the region. Sarkar et al. (2007) hypothesized that the reflectors observed in the seismic sections traversing the epicentral region represent anastomosing shear zones created within a highly compressive stress regime. This observation of high reflectivity, together with a high Poisson's ratio (Kayal et al., 2002; Mishra and Zhao, 2003) in the hypocentral region could indicate enhanced fluid concentrations in a highly sheared zone (Mishra and Zhao, 2004).

Although seismological studies have been carried out for deciphering the source parameters of the Anjar earthquake, there is very limited subsurface information from the southern Kachchh region that hosts this earthquake and the causative mechanism of the high intensity event. In the present work, we carried out MT investigations to image the deep crustal architecture of the region and understand the seismogenesis. The MT results are integrated with the seismicity and seismic velocity structure for better understanding the electrical resistivity structure of the crust.

Geology and tectonics of the study region

The important structural features that played a vital role in the geological evolution of the Kachchh rift basin include a group of E-W trending faults, six major highlands surrounded by a residual depression and plains of the Great Rann (Fig. 1). The six major uplifts namely Pachcham, Khadir, Bela, Chorar, Wagad and Kachchh Mainland (KM) occur along three sub-parallel E-W fault lines (Fig. 1). The E-W trending primary faults from north to south are the: (1) Nagar Parkar fault (NPF) (2) Island Belt fault (IBF) (3) Kachchh mainland fault (KMF) in the middle of the basin and (4) North Kathiawar fault (NKF) at the southern limit of the basin. In addition to these, other faults namely, the South Wagad Fault, North Wagad Fault, Gedi Fault, Katrol Hill fault, Banni Fault, Vigodi Fault (Biswas, 2005, 2016; Pavan Kumar et al., 2017) exist in the region. The Mesozoic rocks ranging in age from Middle Jurassic to lower Cretaceous are exposed extensively in the major uplifts. The Tertiary rocks are seen along the coastal belt of the southern and the western Kachchh bordering the Mesozoic rocks. The KM is divided into northern and southern parts by the E-W trending KHF (Thakkar et. al., 1999; Bhattacharya et al., 2013), which marks a sharp lithotectonic contact between the Cretaceous and the Jurassic rocks.

MT field survey and data processing

The broadband (period 0.01-1000s) MT data is acquired from 21 sites along a ~NE-SW profile that traverses the KHF, SWF and KMF (Fig. 1). At each site, the recording is done for 3-4 days using a ~~M/s Metronix~~ data acquisition system from Metronix (GmbH, Germany) comprising a data logger

(ADU-07), Pb-pbcl2 electrodes and magnetic induction coils (MFS-06e). The electric dipole length was in general 80 m but at a few sites it was between 70 and 80 m. The MT time series is then processed and the earth response functions, namely impedance tensor, ~~phases~~ and tipper vectors are estimated for the whole period range. The time series are processed using commercial MT data processing package 'MAPROS (M/s Metronix GmbH, Germany). The selective stacking method was used to estimate impedance tensors. The processing of MT data and extraction of transfer functions from the timeseries involves a sequence of pre-processing steps such as: preconditioning of the data, transformation from the time to the frequency domain, and estimation of transfer functions. The timeseries data of each of the electric and the magnetic field components were manually edited by identifying and rejecting the bad segments containing spikes before conversion into the frequency domain. The impedance tensors represented as apparent resistivity and phase curves are shown in figure 3, for 9 sites. After calculating the tensor elements in the measurement coordinate system, the last step in the processing procedure is determination of the principle coordinate system. The rotation angle for this purpose can be obtained by minimizing the diagonal elements (Z_{xx}, Z_{yy}) of the impedance tensor. MT transfer functions that contain information about the dimensionality of the subsurface structures are sensitive to noise and can contain distortions due to localized 3D near-surface conductors, galvanic distortions, current channelling, geological and cultural noise. The distortions of regional electric field by local structures are arguably the greatest bane of MT method and affect the quality of interpretation. Therefore, removal of these distortions and recovery of the responses related to the regional structure is necessary before inverting the acquired data for subsurface conductivity distribution. In general, the subsurface structure is more complex than a simple 1-D layered model. For regions having structures with preferred geological strike, MT data can be interpreted in terms of 2-D models and the regional strike of the subsurface structures can be estimated from the observed data. We analysed the data using two methods, the first one formulated by Becken and Burkhard (2004) (hereafter termed as BB approach) and second one by Caldwell et al. (2004), known as the phase tensor (PT) analysis.

The BB technique is based on the electric polarization states and ellipticity criteria of telluric currents. According to the technique, interaction of a linearly polarized homogeneous external magnetic field with a regional 2-D conductivity anomaly will project secondary elliptically polarized magnetic fields. When small scale inhomogeneities galvanically distort the electric fields, the ellipticity remains unchanged but changes in field rotations and amplifications are observed. Thus, by vanishing the ellipticities of the electric and magnetic fields, the regional strike direction can be identified, even in the presence of distortion. The advantage of the BB- analysis is that, it uses a full eight parameter description of the impedance tensor and thereby avoids possible bias in strike angle

estimation and regional impedances. Caldwell et al. (2004) have defined a phase tensor, $\Phi = X * Y^{-1}$, where X and Y are the real and imaginary components of the impedance tensor which are unaffected by galvanic distortions in the observed MT data. Therefore, rotation of the tensor to get the coordinate invariant principal components (Φ_{min} , Φ_{max}) gives the strike direction with a 90° ambiguity. The phase tensor (PT) approach does not invoke any assumption about the dimensionality of the regional conductivity structure and enables robust estimates of distortion parameters and regional strike.

We first performed the distortion analysis on the observed data using the BB method. In case of a pure two-dimensional (2-D) medium, the ellipticities of the impedance tensor that do not depend on the direction of the inducing field will vanish in the regional strike direction. The distortion parameters, the ellipticities and the corresponding distortion angles for some sites are shown in supplementary information (SI). The Galvanic distortion analysis using the BB decomposition technique results in very small values of the ellipticities (close to zero) for the telluric vectors (e_x , e_y) and low and non-variable distortion angle for majority of sites. The conditions for regional two-dimensionality require that the distortion angles at each site should be constant over a period (Becken et al., 2008). The distortion angles and ellipticities of the telluric vectors broadly affirm the validity of 2-D approximation of the data except at few sites, in the southern part of the profile, where moderate 3-D effects are observed, in terms of non-vanishing ellipticities and variable distortion angles. We estimated the regional strike direction in a broad frequency range (100Hz-1000s) using the distortion corrected impedances at all the sites. We also estimated the strike direction in four period bands (0.1-1s, 1-10s, 10-100s and 100-1000s) for each site (maroon colour bars in figure 4). The rose diagram showing the strike values obtained using the single site multifrequency approach, for the period range of 0.1-1000s, is shown figure 5a. The multisite multi frequency mode (MSMF) analysis results in a regional strike of N61°E for a broad frequency range of 0.1-1000s. The dominant E-W strike direction revealed by the rose diagram and estimates from the MSMF mode analysis, coincides with the Precambrian Delhi –Aravalli trend prevailing in this region, strikes of the surface level geological trends and major faults. To constrain the geoelectric strike, which has an inherent 90° ambiguity, we plotted the direction of the inductions vectors (Tippers) in the period range of 1-1000s (Fig 5b). The orientation of the real induction vectors, shown in Fig.5b, also reveal a dominant E-W strike supporting the Precambrian Delhi-Aravalli trend for the region.

Further, the phase ellipses in four different periods (1s, 10s, 100s, and 500s) obtained from the PT analysis are shown in figure 4. The major axes of the ellipses are broadly aligned in the N-S direction (E-W, if we consider the 90° ambiguity) at all the periods. We analysed the distortion parameters (skew angles, Φ_{min} and Φ_{max}) and estimated the strike values (Fig. 4) at four periods (1,

10,100, and 1000s). The phase ellipses at high frequencies show dominant circular shapes indicating homogeneous 1-D/2D structures at shallow levels. The smaller skew values observed for most of the sites suggest negligible presence of galvanic distortions. However, it is interesting to note that the phase ellipses in the 10s period are highly distorted with large skew values, particularly between the KMF and the KHF. This is indicative of a highly heterogeneous nature of the upper crust. It is worthwhile to note that the hypocentral depth of the 1956 Anjar earthquake is at a depth of 15km. Further, the phase ellipses show moderate distortion between 100s and 1000s period. High skew values (± 20) are observed in the close vicinity of the SWF, KMF and KHF zones in these periods. Nevertheless, the majority of phase ellipses are oriented in the N-S or E-W direction for all the periods, consistent with the estimates from the BB technique, considering the 90° inherent ambiguity (Fig. 4). The static shift effects (Simpson & Bahr 2005) are less prominent in the present data set since the region comprises of thick conductive sediments (2-3km). The minor static shifts were corrected by comparing the apparent resistivity values of the adjacent stations (Chandrashekar et al., 2012) before implementing the 2-D inversion scheme. Using the estimated geoelectric strike, the regional 2-D impedance tensor at each site is decomposed and rotated into the respective traverse electric (TE) and transverse magnetic (TM) modes. Now, N61E is the TE mode and N29W is TM mode, as the N-S and E-W are the measuring direction for -xy component and yx- components respectively.

In order to estimate the maximum depth of penetration at each site along the profile, the Niblett–Bostick depth approximation method (Niblett and Sayn-Wittgenstein, 1960; Bostick, 1977; Jones, 1983) is applied to the dataset. The penetration depths are dependent both on the electrical resistivity of the subsurface and maximum time period recorded at each individual site. In this method, the depth of penetration is determined by the period and subsurface conductivity/resistivity. This approach is valid only if 2-D transverse electric (TE) and transverse magnetic (TM) modes are fully decoupled in the orthogonal directions and penetrate to the same depth as the 1-D signals (Jones, 2006, Danda et al., 2020). The estimated depths of penetration at every site for the two modes (TE- and TM-) are shown in Fig.6. It can be seen that the depth of penetration at majority of the sites is > 50 km in either of the modes. Therefore, this data set can be effectively used image the crustal structure of the Anjar seismic zone.

Two-dimensional (2D) modelling

The distortion-corrected and rotated impedance tensors are inverted to obtain a two-dimensional (2D) crustal geoelectric structure along the profile. The nonlinear conjugate gradient (NLCG) 2D inversion algorithm of Rodi and Mackie (2001) in-built in the MT interpretation package, WinGLink (M/s Geosystem SRL, Italy) is used for this purpose. The NLCG algorithm provides regularized solutions for non-quadratic optimization problems by minimizing an objective function which is a weighted sum of normalized data misfits and smoothness of the model (Rodi & Mackie 2001). The

technique of the conjugate gradients was developed by Hestenes & Stiefel (1952) to solve a linear system of equations $Bx = y$ for sparse matrices B . The underlying principle is to find a set of orthogonal directions and to compute accompanying weights in a manner that every search direction is used only once. As a result, convergence is generally fast compared to steepest descent equation solvers. This technique has been used for non-linear minimization problems by Fletcher & Reeves (1959) and for inversion of magnetotelluric (Mackie & Madden, 1993; Rodi & Mackie, 2001). Conjugate gradient method uses updated model vectors which are conjugate versions of each successive gradient vector, i.e. the directions of updates are not specified a-priori but are determined sequentially as linear combinations of previous direction vectors. Use of these conjugate directions helps the minimization procedure to make uniform progress towards convergence which is not so important in quadratic problems but can be crucial importance in non-quadratic problems (e.g. non-linear inversion). NLCG method yields an alternative minimization a nonlinear function directly without making any assumptions about its linearity.

We considered the starting model as a homogeneous half-space of $100\Omega\text{m}$ resistivity and assigned an error floor of 20% for TE-mode apparent resistivity, 10% for TM-mode apparent resistivity, 01.% for Hz component and 5% for TE- and TM-mode impedance phase. A large error floor for apparent resistivity compared to the impedance phase reduces the influence of static shift. Thiel et al. (2009) have shown that the MT response along the strike of the 2-D structure (i.e. TE-mode for 1 2-D case) would be affected by charge accumulations on either side of the conductive sediments. We, therefore, set a large error floor for the TE-mode apparent resistivity. Becken *et al.* (2008) have also demonstrated through a synthetic model study that downweighting of TE-mode apparent resistivity helps in minimizing 3-D effects when the data are interpreted for 2-D structures. They showed that downweighting of TE-mode apparent resistivity data even takes care of the strong 3D effects in the observed data while interpreting in terms of 2-D (Ogawa, 2002). We have not included the topography of the Next, we have not included the topography in the inversion process since majority of MT stations laid on a topography topographic range of $\sim 50\text{--}200$ m and the effects arise in the 2D inversion processes due to this topographic range is negligible (Kumar and Manglik, 2011). An appropriate value of the regularization parameter (τ) is needed to achieve a tradeoff between the RMS error of the misfit and smoothness of the model. We executed a number of model runs for different values of τ ranging between 1 and 100 and iterated the solution until it converges and stabilizes with no further significant reduction in the RMS error of misfit. A tradeoff curve between the RMS error and model roughness suggests an optimum value of τ equal to 7 for the detailed inversion process. We performed a combined inversion of TE, TM modes and Hz data to obtain the geoelectric structure of the subsurface.

After 80 iterations, the RMS error (2.62) remains stable with no further decrement. To check the robustness of individual features obtained in the model, we performed a constrained inversion mimicking the procedure followed by Li et al. (2003) and Pavan Kumar et al. (2014, 2017). During the constrained inversion, we replaced the resistivity of the feature, that needs to be checked for the robustness with the half space resistivity value and re-executed the inversion process with similar inversion parameters as earlier. In a similar manner, we checked the robustness of the various features (marked as C1 to C3 and R1-R6 in figure 7) observed in the obtained model. The results of this constrained inversion and the respective RMS errors are shown in SI. From the analyses it is evident all these features are reproduced with little change in their geometry. Further, to check the robustness of conductor C1, we performed a forward modelling test, in which we masked the feature with a surrounding resistivity and estimated the forward response at a site above the feature. The forward modelling responses with and without the conductor (C1) are shown in SI. The result indicate a significant misfit between the observed and the calculated responses at higher periods without the conductor, which also indicate the robustness of the deeper level conductor. Finally, we selected a model (Fig. 7) among all the constrained inversion models that best fits the observed data. The resultant sensitivity map and the RMS error at each site are also shown in the figure 7. The sensitivity matrix is a real matrix with one row for the real dataset and the next for the imaginary data. The values are calculated by summing up the absolute values column wise of the error-weighted sensitivity matrix using the code of Mackie *et al.* (1997). These sums are normalized by cell area and assigned to the respective grid elements. The structures with sensitivity matrix values of above 0.0001 are considered to be resolved features (Brasse *et al.*, 2002; Ledo & Jones, 2005). A large value of the sensitivity parameter (red, yellow, and green colors) indicates a well-resolved region. It is evident that major features in the model are associated with moderate to high sensitivity values. The pseudo section depicting the fit between the observed and calculated data (apparent resistivity and phase) along with the real and imaginary Hz components are shown in figure 8.

Results and Discussion

The 2-D geoelectric section along the profile (figure 9) reveals many conductive and resistive zones (marked as R1-R3, C1-C4) in the upper and the mid crustal levels suggesting a strong heterogeneous electrical resistivity structure. The top high conductive layer ($\sim 10 \Omega.m$) with a thickness of 2-2.5km represents recent to Mesozoic age sediments overlain on the Precambrian basement. It is interesting to note that the thickness of the sediments decreases considerably in the southern and central portions of the profile suggesting variable basement configuration in the region. Moderate resistivity values at

shallow depths in the southern part of the profile might reflect the presence of exposed Deccan basalts in this region.

The present profile is the southern extension of the MT profile presented in Pavan Kumar et al. (2017). A highly resistive vertical zone ($\sim 5000 \Omega.m$) observed in the southern portion of their profile coincides with the resistive zone (R1) observed in the northern end of the present profile (Fig. 8). This high resistivity zone indicates a mafic intrusion in the Kachchh rift basin that has also been inferred by the seismological and the gravity studies (Chandrashekar et al., 2009; Rao et al., 2015). In addition to R1, the model reveals two more moderate resistive zones (R2 & R3) in the mid to upper crustal levels. The seismic section along Anjar –Bhachau (Sarkar et al., 2007) shows strong reflections at upper to mid crustal depths ($\sim 5, 10$ and 18km) including those at the top of the lower crust ($27\text{--}29\text{ km}$). The reflectors observed in their sections are superimposed on the 2-D resistivity sections (Fig. 8). Coincidentally, some of these strong sub Moho reflectors match well with the top of the resistivity zones (Fig. 8) supporting our view that these resistivity bodies indicate the presence of crustal level intrusions in the rift basin.

Upper mantle conductor

The geoelectric section of the eastern Kachchh produced by Pavan Kumar et al. (2017) delineated a high conductive zone in the upper mantle (C1 in their figure 3), in close vicinity of the Moho, was interpreted as the zone of an upper mantle fluid reservoir. Similar to their results, the present geoelectric section (Fig. 8) also delineated a high conductive zone, C1 ($\sim 1 \Omega.m$) in the upper mantle depths, suggesting the presence of a fluid reservoir. These fluids filled zones might possibly reflect the presence of lithospheric-scale weak zones beneath the Kachchh region that apparently serve as channels for asthenospheric upwelling (Yin et al., 2017, Sharma et al., 2018). In continental rifts and regions affected by mantle plumes, magmatic underplating is prevalent and represents ponding of the upwelling magma due to the density contrast in the vicinity of the Moho. It is suggested that the injection of the magma at the base of the crust can take place in the form of a series of sills that get differentiated into gabbroic and ultramafic rocks at the upper and lower levels (Cox, 2002, Sharma et al., 2018). This implies that in volcanic regions, underplating plays a dominant role in the tectono-magmatic evolution of the crust and the lithosphere. The zone of the upper mantle reservoir/asthenospheric upwelling may result in lower crustal decoupling and inhomogeneous stress distribution due to fluid pathways, resulting in the upliftment of various tectonic blocks (Fig. 1b) within the basin. Mandal and Pandey (2010) inferred a massive emplacement of partially molten hydrated magmatic material at the bottom of a weak, ductile, and sheared lower crust during the earlier episodes of rifting and thermal upwelling, which lowered the depth of the mantle solidus. They further postulated that the observed marked thinning of the crust and the asthenosphere below the central

Kachchh rift zone, could be a result of interaction between the lithosphere and Deccan–Reunion mantle plume (Mandal, 2016).

We superimposed the surface location of the major faults, i.e. KMF, BF and KHF on the resistivity section (Fig.8). It can be seen that these fault zones are associated with conductive zones at deeper levels. One of the significant differences between this section and that beneath the seismically active Wagad region (Pavan Kumar et al., 2017) is that, unlike the SWF, which transects the entire crust and reaches the upper mantle levels, connecting the fluid reservoir to the mid to lower crustal depths, the present section does not provide any evidence of deep-rooted fault systems (either the KMF or KHF). These faults do not cut the entire crust and rather terminate at mid-crustal depths (15-18km).

We superimposed the 3-D relocated hypocentres of ($M \geq 3.0$) earthquakes that occurred during 2006-2017 (Pavan Kumar, 2017), determined using waveforms recorded by the ISR seismic network (Chopra et al., 2008), on the geoelectric section. For an accurate correlation of the seismicity patterns with the resistivity features, we only projected the events that lie within 5km on either side of the profile. It is interesting to note that most of these events are at the boundary between the resistive and conductive zones, representing the subsurface expression of SWF and KMF. Few events are located near the feature C3.

Mid crustal resistors and conductors in the Kachchh intraplate region

The principal features in the model are the presence of a mid to upper crustal conductor (C2) and an apparently U-shaped high conductive zone (C3) in the upper and middle crust (<18km depth), north of the KHF and south of the KMF, within the KMU, respectively. These conductive zones, C2 and C3 are separated by the high resistivity zones (R1, R2 & R3) interpreted as the crustal level mafic and basaltic intrusions. Wannamaker et al. (2002) have delineated a U-shaped mid to lower crustal conductor beneath Southern Alps of the central South Island of New Zealand. They linked such geometry of the conductor with fault-controlled fluid movements. The surface location of zone C2 demarcated in this study, matches well with the KMF. We therefore infer that the enhanced linear conductive zone C2 may represent the electrical image of a major fault/fracture zone at a crustal scale (at a depth of ~15km). Another conductive zone C3, shallows to the northeast and approaches the surface near the geological boundary of the Tertiary and the Mesozoics, 5–10 km east of the Bhuj Fault (Fig. 1). The top of the concave upward lies at 18 km. The conductor does not continue south, instead it shallows near the KHF zone and is surrounded by crustal intrusives. Most of the geological (Karmalkar, 2008) and geophysical studies suggest underplating of high-density material in the Kachchh-Saurashtra-Cambay region formed by lithospheric melting and injection into the lower crust during the rifting (Rao et al., 2015), which indeed suggests presence of trapped basaltic magmas at the base of the crust or within the crust.

Gravity data are also acquired in the southern Kachchh region at a station interval of ~ 1 km or less, along the available roads and tracks, using a CG 5 gravimeter having an accuracy of 0.01 mGal. To ensure high quality data, the elevation and position of each gravity station are determined based on a Real Time Kinematics survey conducted using a Leica Geosystems instrument having an accuracy of 10 cm. Theoretical gravity values at each station are calculated from the Geodetic Reference System 1967 (GRS67) gravity formula. The Bouguer gravity anomaly (BGA) is obtained after applying all the necessary corrections (drift, latitude, free-air and Bouguer correction) using a Bouguer slab of density 2.67 gm/cc and plotted along the profile (Fig. 9). The BGA values suggest low densities (negative BGA) in the central portion of the profile with positive BGA (high dense material) in the southern and northern ends, supporting the high and low conductive zones respectively, observed in the MT model.

Mid-crustal conductors and source of fluids:

According to Frost and Bucher (1994), there are five ways by which fluids can be intruded into the crust. These include gravity-fed water, passive mantle degassing, water of metamorphic origin, magmatic water and tectonic water transport and redistribution. Further, it has been suggested that these fluids can originate due to meteoric and/or igneous processes occurring at shallow depths, whereas carbonic fluids of mantle origin are driven towards the lower crust (Frost and Bucher, 1994). In an intraplate setting, one of the potential sources of fluids is the metamorphic fluid generated by dehydration of minerals during prograde metamorphism. Several studies have postulated that fluids in the lower crust are of metamorphic origin (Borevsky et al., 1987; Stanley et al., 1990; Bailey, 1990). This is a possible source because weakly metamorphosed sediments, hydrothermally altered basalts, and serpentinites contain significant amounts of water bound up in silicates. Magmatic water can be produced by the crystallization of igneous melts. In addition, fluids may get trapped in pore spaces as sedimentary formation brines and downward circulation of meteoric water (Kerrick et al., 1984). An elementary analysis based on the seismogenic zone depth and experimental rheological constraints (Wannamaker et al., 2004; Cannolly and Podladchikov, 2004) indicates that tectonically induced buoyancy would cause fluids to accumulate below the brittle-ductile transition zone (BDTZ). Trapping of fluids at mid-crustal levels, particularly at the BDTZ is reported from various active regions of the world (Bailey, 1990; Kennedy et al. 1997, Ritter et al., 1999; Jiracek, 1999; Ogawa et al. 2001; Cannolly and Podladchikov, 2004; Becken and Ritter, 2012). Granitic magmas are also a source of fluids released during their crystallization (Burnhan, 1979, Frost and Bucher, 1994). Mandal and Pandey (2011) have estimated the temperature -depth profiles within the KRB that reveal a shallow and deeper BDT zones at 14 and 34 km depth (in vicinity of Moho), respectively Pavan Kumar et al. (2017) have also reported trapped fluids in the north-eastern part of the Kachchh region at the BDTZ (15-

18km) that are associated with the Gedi fault zone. It is suggested that fluids are widely distributed within the crust and the upper mantle and their behaviour in the seismic source region might have controlled the nucleation and rupture process of the 2001 Bhuj earthquake (Pavan Kumar et al., 2017). The existence of aqueous fluids within and below the seismogenic layer could affect the long-term structural and compositional evolution of fault zones, change the strength of the zones, and alter the local stress regime (Sibson, 1992; Hickman et al., 1995, Umeda et al., 2011).

Glazner and Ussler (1988) suggested that mid-crustal increase in seismic P-wave velocities indicate the upper boundary of magma bodies. They further inferred that near-liquidus basalts should be less dense than the crust where the mid-crustal velocity increases and denser above them. Due to the sharp density interface at mid-crustal depths, the rising mafic magma may be trapped where it loses buoyancy and hence localises in a small depth interval in the crust. To estimate the variation in seismic velocities in the study region, we plotted one dimensional V_p values (Chopra et al., 2014) and respective densities (calculated from the empirical relationship between V_p and density given by Brocher, 2005) as a function of depth at 3 sites, namely BHI, BAN and DUI, which are in close vicinity of the sites where the MT data is acquired (Fig. 1 & 10). The 1-D velocities are computed using receiver functions (Vinnik, 1977), which is a conventional technique for studying the seismic velocity structure of the crust and upper mantle beneath seismic stations. The amplitude and timing of the composite P-to-S converted waves can be modelled to determine the velocity structure. Chopra et al. (2014) applied the receiver function technique on the teleseismic seismograms recorded by a network of 32 broadband seismographs spread all over Gujarat state. It is observed that station BHI is underlain by low V_p values, which suddenly increase in the depth range of 15 to 18km, with a corresponding increase in the crustal density values. The low V_p and low densities are well correlated with a high conductivity zone (C3) in the MT model. The seismic station BAN located on the northern side of the profile is associated with very high V_p values at shallow depths and the corresponding density ranges suggest presence of intrusives from mantle depths, delineated as a very high resistivity zone in the MT model (Fig. 9). The seismic station DUI to the south of KMF shows V_p values in between those found beneath BHI and BAN. The narrow density interface observed at the BHI site could probably be acting as a channel (Glazner and William, 1988) to converge the mantle derived heat to form a zone of trapped magma. It is possible that exchange of heat with the underplated material may release carbonate fluids and/or result in dehydration of minerals, resulting in partial melting and release of large amounts of H_2O & CO_2 fluids upon crystallization (Frost et al., 1989; Wannamaker et al., 1997; Bolongo et al., 2013, Mandal, 2016). This fluidized zone is thus reflected as a high conductive zone in the resistive model (Fig. 9). We therefore postulate that the conductive anomalies (C2 & C3), C3 in particular,

may be attributed to a zone of trapped carbonate fluids probably representing fluids originally trapped or newly generated by dehydration in this active intraplate setting.

Role of trapped fluids and crustal heterogeneity in generating the 1956 Anjar earthquake

We superimposed the hypocentres of the 1956 Anjar earthquake (marked as stars) estimated by Chandra (1977) [23.0°N, 70.0°E] and Chang and Gao (1995) [23.3°N, 70.0°E] on the 2-D electrical section (Fig. 8). Interestingly, these two locations fall on either side of the resistive zone R2, which is interpreted as a basaltic intrusion, precisely, at the resistive (R2) – conductive (C2 & C3) transition zone at 15km depth. The features C2 and C3 are interpreted as mid to upper crustal fluid rich zones. Tauzin et al. (2017) have suggested that fluid circulation in the crust is highly dominated by fault zones separating blocks of crustal material and these zones can act as favourable routes for the escape of fluids, thus triggering small to moderate sized earthquakes in a region. Further, Yin et al. (2017) inferred that micro-earthquakes mainly distribute along the brittle-ductile transition zone, reflected as a contrast between the resistive and the conductive zones or the high pore pressure fault zones. They also opined that epicentres of big destructive events occur near significant rheological anomalies. Considering the association of seismic distribution and hypocentre(s) of the Anjar earthquake with the transition zone, we infer that the presence of trapped fluids and their seepage to the resistive/strong parts of the crust might be a possible cause for the triggering of the 1956 event as well as the current seismic activity in the region. Significant crustal heterogeneity, manifest in terms of contrasts in electrical resistivity, might indicate variations in the rheological strength of the crustal rocks, which are also evidenced in various seismic tomographic sections and potential field observations. However, most of the rift zones have low rheological strength (low resistive zones) that are inferred as fault/shear/weak zones. In conjunction with a high conductive anomaly at upper mantle depths, the crustal scale rheological heterogeneity might play a vital role in the seismotectonics of the Kachchh rift basin.

Genesis of seismicity in the Kachchh intraplate region:

Lio and Kobayshi (2002) have presented a broad description of the physical understanding of intraplate earthquakes with special reference to the Japanese Islands. They inferred that geometry of the faults could play a major role in the occurrence of large magnitude earthquakes in an intraplate region. The seismogenic faults with a downward lower crustal extension could create localized shear deformation across the faults leading to stress accumulation. They further hypothesized that significant increase in local shear deformation would occur before the occurrence of a large magnitude event. They studied a couple of models that dealt with the intraplate earthquake generation processes and argued that a localized shear model with a sudden increase in aseismic slip could explain the generation of intraplate earthquakes. In the context of Kachchh basin, the prominent faults are the KMF, KHF, SWF, NWF,

GF, IBF and ABF, with NKF and NPF as the rift basin boundaries. Many geophysical studies, particularly MT (Sastry et al., 2008, Chandrashekar et al., 2012, Naganjuneyulu et al.2010; Pavan Kumar et al.2017; Kapil Mohan et al. 2018) are carried out in the region to map the sub-surface expression of these faults. These studies provided electromagnetic images of these fault systems except for IBF, NKF and NPF, where surveys are difficult since the areas are water logged most of the time. A cartoon showing the geological interpretation of results from the present MT study and previous geophysical studies (Pavankumar et al., 2017, 2019; Sharma et., 2018) is shown in figure 11. From MT results, it is observed that among all the faults, only SWF has a downward extension to upper mantle depths (40-45km) and possibly meets the upper mantle fluid reservoir inferred by Pavan Kumar et al. (2017). It is to be noted that two large earthquakes, namely the 1819 Kachchh (M 7.8) and the 2001 Bhuj earthquake (Mw 7.7) have occurred in the region, in addition to the 1956 Anjar earthquake (Mw 6.0, depth ~15km). However, the source parameters of the 1819 earthquake are still ambiguous since the earthquake has occurred during the non-instrumental time and there is no geophysical data available for this event. Nevertheless, the 2001 earthquake (depth 25km) is well studied by various researchers and it is observed that the hypocentral zone of the 2001 main shock is characterized as a fluid saturated zone with the rooting of NWF onto the SWF (Pavan Kumar et al., 2017). Pavan Kumar et al., (2019) suggested that the 1819 event is associated with the south dipping NPF and the ABF might be a listric synthetic splay of the basin margin indicating the ongoing Holocene deformation in the region. Considering the hypothesis of *Local stress model* proposed by Lio and Kobayshi (2002), we suggest that SWF could be the main seismogenic fault in the region that can accumulate maximum shear stress in the lower crustal depths and produce large magnitude earthquakes. The presence of a mantle fluid reservoir and the subsequent mantle flow play a key role in the style of lower crustal deformation through stress accumulation in the upper crust. Among the proposed distributed pure shear models (McKenzie, 1978) and the localized simple shear models (Wernicke, 1981) for a rift zone, we suggest that the basal drag model with localized simple shear, where the seismogenic SWF cuts the entire crust, could explain the occurrence of large magnitude earthquakes in this active intraplate region. Supporting the hypothesis, the KMF, KHF and the GF do not have deep downward extensions and probably have less chance of generating large magnitude earthquakes. The zone of asthenospheric upwelling in the Kachchh region is also evidenced by the present as well as previous geophysical studies. The resulting drag force generates lower crustal coupling and inhomogeneous distribution of stress (Yin et al., 2017) thereby uplifting various tectonic blocks within the Kachchh rift basin.

Conclusions:

Results from magnetotelluric (MT) investigations in the south-eastern part of the Kachchh region reveal a highly heterogeneous crustal structure, particularly in and around the hypocentral zone of the

1956 Anjar earthquake. The geoelectric section presented in this study affirms the presence of an upper mantle fluid reservoir beneath the Kachchh region. In contrast to the SWF, the KMF is confined to upper crustal depths and is associated with a highly conductive fluidized zone. Importantly, the model delineated a U-shaped conductive zone bordered by high resistive crustal intrusives between the KHF and BF. We hypothesize that the conductive zone with trapped aqueous fluids experienced a tectonically induced buoyancy causing upward movement of these fluids. Further, in conjunction with seismicity data, we postulate that seepage and/or escape of the trapped fluids in the region could lead to increase in stresses thereby generating the 1956 Anjar earthquake and moderate to low magnitude earthquakes in this intraplate region.

Acknowledgements:

We thank the Director General, ISR for kind support and encouragement. GPK thank the Director, CSIR-NGRI and PM thank Director, NIO for the permission to publish the present work. We also thank Prof. M. Becken for providing his distortion analysis code. We thank Mr. Himanshu Chaube for help in MT field investigations. We are grateful to the two anonymous reviewers for their comments and suggestions which significantly improved quality of the manuscript. We shall deposit the data in a public domain/ in an appropriate repository after acceptance of the manuscript.

References:

1. Bailey, B.C., Trapping of Aqueous fluids in the deep crust, *Geo. Phys. Lett.*,17(8), 1129-1132, 1990
2. Becken, M. and Burkhardt, H., An ellipticity criterion in magnetotelluric tensor analysis, *Geophys. J. Int.*, 159, 69–82, 2004.
3. Becken, M., Ritter, O., Park, S.K, Bedrosian, P. A, Weckmann, U. and Weber, M., A deep crustal fluid channel into the San Andreas Fault system near Parkfield, California. *Geophys J. Int.*, 173(2), 718–732, 2008.
4. Bhattacharya, F., Rastogi, B.K., Mamata Ngangom, Thakkar, M.G. and Patel, R.C., Late Quaternary climate and seismicity in the Katrol hill range, Kachchh, western India, *Journal of Asian Earth Sciences*, 73, 114–120, 2013.
5. Bilham, R., Slip parameters for the Rann of Kachchh, India, 16 June 1819, earthquake, quantified from contemporary accounts. In Stewart, I. S. & Vita-Finzi, C. (Eds) Coastal Tectonics. *Geological Society London*, 146, 295-318, 1999.
6. Biswas, S.K., A Review of Structure and Tectonics of Kutch Basin, Western India, with special reference to Earthquakes. *Current Science*, 88(10), 15, 1592-1600, 2005.
7. Biswas, S.K., Regional tectonic framework, structure and evolution of the western continental marginal basins of India. *Tectonophysics*, 135,307-327, 1987.

8. Biswas, S.K., Tectonic Framework, Structure and Tectonic Evolution of Kutch Basin, Western India. *Special publication of the geological society of India*, 6, 129-150, 2016
9. Bolongo M S, Nunes H O, Padilha A L, Vitorello I and Padua M B 2013 Anomalous electrical structure in the northwestern Paraná Basin, Brazil, observed with broadband magnetotellurics; *J. S. Am. Earth Sci.* 42 74–82.
10. Borevsky, L.V., Vartanyan, G.S. and Kulikov, T.B., 1987. Hydrogeological essay. In: Y.A. Kozlovsky (Editor), *The Superdeep Well of the Kola Peninsula*. Springer Verlag, Berlin, pp. 271-287
11. Brasse, H., Lezaeta, P., Rath, V., Schwalenberg, K., Soyer, W., Haak, V., 2002. The Bolivian Altiplano conductivity anomaly. *J. Geophys. Res.*, 107 (B5), 2096
12. Brocher, T. M., Empirical Relations between Elastic Wave speeds and Density in the Earth's Crust. *Bulletin of the Seismological Society of America*, Vol. 95, No. 6, pp. 2081–2092, 2005.
13. Burnham, C. W., *Magma and hydrothermal fluids, Geochemistry of hydrothermal ore deposits*, Barnes, H. L., ed., 71-136, New York, Wiley Intersci., 1979.
14. Caldwell, T.G., Bibby, H.M. & Brown, C., The magnetotelluric phase tensor, *Geophys. J. Int.*, 158, 457–469, 2004.
15. Calignano, E., Sokoutis, D., Willingshofer, E. Gueydan, F. and Cloetingh, S. Asymmetric vs. symmetric deep lithospheric architecture of intra-plate continental orogens. *Earth Planet. Sci. Lett.*, 424, 38-50, [10.1016/j.epsl.2015.05.022](https://doi.org/10.1016/j.epsl.2015.05.022), 2015.
16. Chandra, 1977. Earthquakes of peninsular India--a seismotectonic study, *Bulletin of the Seismological Society of America*. 67(5), 1387-1413, 1977.
17. Chandrasekhar, D. V, Burgmann, R., Reddy, C.D., Sunil, P. S. & Schmidt, D. A. Weak mantle in NW India probed by geodetic measurements following the 2001 Bhuj earthquake. *Earth Planet. Sci. Lett.*, 280, 229–235, 2009
18. Chandrasekhar, E., Mathew, G. and Harinarayana, T. A new hypothesis for the deep subsurface structures near the Bhuj 2001 earthquake (Mw 7.6) hypocenter zone and its tectonic implications. *Geophys. J. Int.*, 190, 761–768, 2012.
19. Chopra, S., Tao-Ming Chang, Sowrav Saikia, R.B.S. Yadav, Pallabee Choudhury and Ketan Singha Roy. Crustal structure of the Gujarat region, India: New constraints from the analysis of teleseismic receiver functions. *Journal of Asian Earth Sciences*. 96. 237–254, 2014.
20. Choudhury, S Chopra, K Singha Roy, J Sharma, BK Rastogi, Revisiting the 1956 Anjar Earthquake in Western India: Empirical Green's Function Approach, *Bulletin of the Seismological Society of America* 107 (2), 592-602
21. Chung, W.P., and Gao, H., Source parameters of the Anjar earthquake of July 21, 1956, India, and its seismotectonic implications for the Kutch rift basin, *Tectonophysics*, 242, 281–292, doi: 10.1016/0040-1951-(94)00203-L, 1995.

22. Connolly, J. A. D. and Podladchikov, Y. Y. Fluid flow in compressive tectonic settings: Implications for mid crustal seismic reflectors and downward fluid migration. *Chemistry and Physics of Minerals and Rocks/Volcanology* doi.org/10.1029/2003JB002822, 2004.
23. Cox, K. G. 1983. Deccan Traps and the Karoo: stratigraphic implications of possible hotspot origins. IAVCEI programme and abstracts of XVIII IUCG General Assembly, Hamburg, 96
24. Cox, S., Fluid flow in mid- to deep crustal shears systems: Experimental constraints, observations on exhumed high fluid flux shear system, and implications for seismogenic processes. *Earth Planets Space*, 54, 1121– 1125,2002.
25. Danda N., Rao C.K., Kumar, A., Rama Rao, P., Subba Rao, P.B.V., 2020. Implications for the lithospheric structure of Cambay rift zone, western India: Inferences from a magnetotelluric study. *Geoscience Frontiers.*, 11, 1743-1454.
26. Duncan, R. A. and D. G. Pyle, Raid eruption of the Deccan Traps at the Cretaceous/Tertiary boundary, *Nature*, 333, 841–843, 1988.
27. Fletcher, R. and Reeves, C.M., 1964. Function minimization by conjugate gradients, *Comput. J.*, 7: 149- 154
28. Frost, B. R and Bucher, K., Is water responsible for geophysical anomalies in the deep continental crust? A petrological perspective. *Tectonophysics*, 231,293-309, 1994.
29. Frost, B.R., Fyfe, W.S., Tazaki, K. and Chan, T., 1989. Grain boundary graphite in rocks and implications for high electrical conductivity in the lower crust. *Nature*, 340: 134-136,1989
30. Glazner, A.F. and Ussler, W., Trapping of magma at midcrustal density discontinuities. *Geophysical Research Letters*, 15(7), 673-675, 1988
31. Hestenes, M.R. and Stiefel, E.L., 1952. Methods of conjugate gradients for solving linear systems, *J. Research Nat. Bur. Standards*, 49: 409-436
32. Hickman, S., Sibson, R and Bruhn, R., Introduction to special section: Mechanical involvement of fluids in faulting. *J. of Geophys. Res.*, 100, B7, 12831-12840,1995.
33. Jin, A. and Aki, K., 1988. Spatial and temporal correlation between coda Q and seismicity in China, *Bull. seism. Soc. Am.*, 78, 741-769. 1988.
34. Jiracek, G. R., Gonzalez. V. M., Caldwell, T. G., Wannamaker, P. E. and Kilb, D. Seismogenic, electrically conductive, and fluid zones at continental plate boundaries in New Zealand, Himalaya, and California, USA. In: Okaya D, Stern T, Davey F (eds) A continental plate boundary: tectonics at South Island, New Zealand, Geophysical Monograph Series AGU, V 175, pp 347–369, 2007.
35. Johnston, A.C. 1996. Seismic moment assessment of earthquakes in stable continental regions-11. Historical seismicity. *Geophys. J. Int.*,125,639-678, 1996.
36. Jones, A. G., 1983. On the equivalence of the “Niblett” and “Bostick” transformations in the magnetotelluric method. *J. Geophysics*, 53:72–73.

37. Jones, A. G., 2006. Electromagnetic interrogation of the anisotropic Earth: looking into the Earth with polarized spectacles. *Phys. Earth Planet Inter.*, 158, 281–291. doi:10.1016/j.pepi.2006.03.026.
38. Kapil Mohan, Peush Chaudhary, Pruthul Patel, B.S. Chaudhary, Sumer Chopra. Magnetotelluric study to characterize Kachchh Mainland Fault (KMF) and Katrol Hill Fault (KHF) in the western part of Kachchh region of Gujarat, India, *Tectonophysics*, 726,43-61,2018.
39. Karmalkar, N.R., Magma underplating and storage in the crustbuilding process beneath the Kutch region, NW India, *Curr. Sci.*, 94, 1582-1588, 2008.
40. Kayal, J.R., Zhao, D., Mishra, O.P., De, R. and Singh, O.P. The Bhuj earthquake: Tomographic evidence for fluids at the hypocenter and its implications for rupture nucleation. *Geophys. Res. Lett.*, 29 (24), 2152, 2002.
41. Kerrich, R., T.E. La Tour, and L. Willmore, Fluid participation in deep fault zones: Evidence from geological, geochemical, and $^{18}\text{O}/^{16}\text{O}$ relations, *J. Geophys. Res.*, 89, 4331-4343, 1984.
42. Ledo, J. and Jones, A., 2005. Temperature of the upper mantle beneath the Intermontane Belt, northern Canadian Cordillera, determined from combining mineral composition, electrical conductivity laboratory studies and magnetotelluric field observations. *Earth Planet. Sci. Lett.* 236: 258-268
43. Li, S., Unsworth, M.J., Booker, J.R., Wei, W, Tan, H. and Jones, A.G., Partial melt of aqueous fluid in the mid-crust of Southern Tibet? Constraints from INDEPTH magnetotelluric data. *Geophysical Journal International*, 153, 289-304, 2003.
44. Lio, Y and Kobayshi, Yoji., A physical understanding of large intraplate earthquakes. *Earth, Planets and Space*, 54, 1001-1004, 2002.
45. Mackie, R., Rieven, S., Rodi, W., 1997. Users Manual and Software Documentation for Two-Dimensional Inversion of Magnetotelluric Data (GSY-USA, Inc., San Francisco, California).
46. Mackie, R.L., Madden, T.R., 1993. Three-dimensional magnetotelluric inversion using conjugate gradients. *Geophys. J. Int.*, 115, 215–229.
47. Mandal, P and Pandey, O.P., Relocation of aftershocks of the 2001 Bhuj earthquake: A new insight into seismotectonics of the Kachchh seismic zone, Gujarat, India. *J. of Geodynamics*, 49(5), 254-260, 2010.
48. Mandal, P. and Pujol, J. Seismic imaging of the aftershock zone of the 2001 Mw 7.7 Bhuj earthquake, India. *Geophys. Res. Lett.*, 33, L05309, 2006.
49. Mandal, P., Variations of seismic velocities in the Kachchh rift zone, Gujarat, India, during 2001–2013. *Tectonophysics*, 672–673, 2016.
50. McKenzie, D. P., Some remarks on the development of sedimentary basins, *Earth Planet. Sci. Lett.*, 40, 25–32, 1978.
51. Mishra, O.P. and Zhao, D. 2003. Crack density, saturation rate and porosity at the 2001 Bhuj, India, earthquake hypocenter a fluid-driven earthquake? *Earth and Planet. Sci. Lett.*, 212, 393-405, 2003.

52. Mooney, W.D, White, S.M. Recent Developments in Earthquake Hazards Studies, IN S. Cloetingh, J. Negendank (eds.), New Frontiers in Integrated Solid Earth Sciences, International Year of Planet Earth, DOI 10.1007/978-90-481-2737-5_6.
53. Morgan, W.J., Hot-spot tracks and the opening of Atlantic and Indian Oceans. In: Emiliani, C., (Eds.) The Sea. Wiley-Interscience, New York, 7: 443-487,1981.
54. Naganjaneyulu, K., Ledo, J.J., Queralt, P., 2010. Deep crustal electromagnetic structure of Bhuj earthquake region (India) and its implications. *Geol. Acta* 8, 83–97.
55. Niblett, E. R., Sayn-Wittgenstein, C., 1960. Variation of electrical conductivity with depth by the magnetotelluric method. *Geophysics*, 25, 998–1008.
56. Ogawa, Y., 2002. On two dimensional modeling of magnetotelluric field data. *Surv. Geophys.* 23, 251–273.
57. Ogawa, Y., Mishina, M., Tadanori G., Hideyuki S., Naoto O., Takafurni K., Yukie T., Tadashi N., Shinya S., Makoto U., Yuji T., Yoshimori H., Masaki M., 2001. Magnetotelluric imaging of fluids in intraplate earthquakes zones, NE Japan back arc. *Geophys. Res. Lett.*, 28, 3741–3744.
58. Pavan Kumar, G., Manglik, A. and Thigarajan, S. Crustal Geoelectric structure of Sikkim Himalaya and adjoin Gangetic foreland basin. *Tectonophysics*. 637, 238–250,2014.
59. Pavan Kumar, G., P. Mahesh, M. Nagar, E. Mahender, V. Kumar, K. Mohan, and M. Ravi Kumar, Role of deep crustal fluids in the genesis of intraplate earthquakes in the Kachchh region, northwestern India, *Geophys. Res. Lett.*, 44, doi:10.1002/2017GL072936, 2017.
60. Pavan Kumar, G., M. Perugu, R. Nikam, M. Nagar, H. Chaube. Magnetotelluric Imaging of Intra-basin Faults in the Kachchh Rift Basin, North-Western India , 2019, IUGG, Montrial -Canada
61. Rao, K.M., Kumar, M. R. and Rastogi, B. K., Crust beneath the northwestern Deccan Volcanic Province, India: Evidence for uplift and magmatic underplating.. *J. Geophys. Res.* 10.1002/2014JB011819, 2015.
62. Ritter, O., Hoffmann-Rothe, A., Bedrosian, P.A., Weckmann, U., Haak, V., 2005. Electrical conductivity images of active and fossil fault zones. In: Bruhn D, Burlini L (eds) In high-strain zones: structure and physical properties, 245, Geological Society of London Special Publications, 165–186.
63. Rodi, W. L. and Mackie, R. L., Nonlinear conjugate gradients algorithm for 2-D magnetotelluric inversion. *Geophysics*, 66, 174–187, 2001.
64. Sarkar D., K. Sain, P.R. Reddy, R.D. Catchings and W.D. Mooney epicentral region, western India Seismic-reflection images of the crust beneath the 2001 M = 7.7 Kutch (Bhuj) epicentral region, western India. *Geological Society of America Special Papers*, 425;319-327, 2007.
65. Sastry, R.S., Nagarajan, N. & Sarma, S.V.S., Electrical imaging of deep crustal features of Kutch, India, *Geophys. J. Int.*, 172, 934–944, doi:10.1111/j.1365-246X.2007.03658, 2008.
66. Sharma, J., Kumar, M. R., Roy, K. S., Roy,P. N. S., 2018. Seismic imprints of plume- lithosphere interaction beneath the northwestern Deccan Volcanic Province. *J. Geophys. Res., Solid Earth*, 123, 10,831–10,853. <https://doi.org/10.1029/2018JB015947>.

67. Sibson, R. H., Implications of fault valve behavior for rupture nucleation and recurrence, *Tectonophysics*, 211,283-293, 1992.
68. Stanley, W.D., Mooney, W.D. and Fuis, G.S., 1990. Deep crustal structure of the Cascade Range and surrounding regions from seismic refraction and magnetotelluric data. *J. Geophys. Res.*, 95: 19,419-19,438
69. Sumer Chopra, R. B. S. Yadav, Hardik Patel, Santosh Kumar, K. M. Rao, B. K. Rastogi, Abdul Hameed, and Sanjay Srivastava Sumer Chopra, R. B. S. Yadav, Hardik Patel, Santosh Kumar, K. M. Rao, and B. K. Rastogi. 2008. The Gujarat (India) Seismic Network, *Seismological Research Letters*, 79(6), 806-815
70. Tauzin, B., Reynard, B., Perrillat, J.-P., Debayle, E., & Bodin, T., Deep crustal fracture zones control fluid escape and seismic cycle in the Cascadia subduction zone. *Earth and Planetary Science Letters*, 460, 1–11. <https://doi.org/10.1016/j.epsl.2016.12.007>, 2017
71. Thakkar, M. G, Maurya, D.M, Rachna, R. and Chamyal, L. S., Quaternary tectonic history and terrain evolution of the area around Bhuj, Mainland Kachchh, western India. *Geol. Soc India*, 53, 601–610, 1999.
72. Thiel, S., Heinson, G., Gray, D. R. and Gregory, R.T., 2009. Ophiolite emplacement in NE Oman: constraints from magnetotelluric sounding, *Geophys. J. Int.*, 176: 753–766
73. Umeda, K., Koichi Asamori, Tateyuki Negi and Tomohiro Kusano, A large intraplate earthquake triggered by latent magmatism. *Journal of geophysical research*, 116, B01207, doi.org/10.1029/2010JB007963, 2011.
74. Vinnik L.P. 1977. Detection of waves converted from P to SV in the mantle, *Phys. Earth planet. Inter.*, 15, 39–45.
75. Wannamaker, P. et al. 2006. Lithospheric dismemberment and magmatic processes of the Great Basin-Colorado Plateau transition, Utah, implied from magnetotellurics. *Geochem. Geophys. Geosyst.*, 9, Q05019.
76. Wannamaker, P.E., Jiracek, G.R., Stodt, J.A., Caldwell, T.G., Gonzlaez, V.M., McKnight, J.D. and Porter, A.D. 2002. Fluid generation and pathways beneath an active compressional orogen, the New Zealand Southern Alps, inferred from magnetotelluric data. *J. Geophys. Res.*, 107, 1-20.
77. Watts A.B. and Cox, K.G., 1989. The Deccan Traps: an interpretation in terms of progressive lithospheric flexure in response to a migrating load. *Earth and Planetary Sciences Letters*, 93, 85–97.
78. Wernicke, B., Low-angle normal faults in the Basin and Range province: nappe tectonics in an extending orogen, *Nature*, 291, 645–648, 1981.
79. Yin, Yaotian, Sheng Jin, Wenbo Wei, Gaofeng Ye, Jian'en Jing, Letian Zhang, Hao Dong, Chengliang Xie, Hongda Liang., Lithospheric rheological heterogeneity across an intraplate rift basin (Linfen Basin, North China) constrained from magnetotelluric data: Implications for seismicity and rift evolution, *Tectonophysics*, 717, 1-15, 2017.

List of figures

Figure 1a: Generalized geotectonic map of the Kachchh region showing the MT sites (magenta diamond symbols). Locations of the three significant earthquakes (Allahbund, Anjar and Bhuj earthquakes) are also shown along with the respective focal mechanisms. The seismic stations and the profile along which Deep Seismic Sounding data are acquired (Sarkar et al. 2007) are shown as triangles and solid line respectively. The solid green lines are the MT profiles of Pavan Kumar et al. (2017). Here, NPF :Nagar Parkar F. IBF: Island Belt F., ABF :Allahbund F. BF :Banni F., KMF : Kachchh Mainland F. Bh F :Bhuj F. , KHF : Katrol Hill F., NWF : Nagar Parkar F., SWF : South Wagad Fault, NKF : North Katiyaware Fault. Figure 1b: Topographic map of the Kachchh region showing locations of the past and historic earthquakes.

Figure 2: Seismicity of the Kachchh region during 2007-17 shown together with the 2001 Bhuj main shock.

Figure 3: Apparent resistivity and phase curves for 9 sites along the profile.

Figure 4: Phase ellipses (for 1s, 10s, 100s and 1000s) obtained from PT analysis and strike directions (bars) estimated from BB approach in the four period bands (0.1-1s, 1-10s, 10-100s and 100-1000s). The minor axes of the phase ellipses are normalized to their major axes to maintain an equal size for the ellipses.

Figure 5: a) Rose diagram obtained after multi frequency single site analysis following the BB approach. The 90° ambiguity of the impedance tensor analysis results in the cross-shaped diagram b) Rose diagram for the induction vectors for the period band of 1-1000s

Figure 6: Niblett-Bostick penetration depths for all sites on the profile. The penetration depths are plotted separately for the TE and TM modes at each site.

Figure 7: (a) 2-D geoelectric structure of the study region (b) corresponding sensitivity map; A large value of the sensitivity parameter (red, yellow, and green colors) indicates a well-resolved region and (c) RMS error shown site-wise

Figure 8: Pseudo sections showing fit between the observed and calculated MT data

Figure 9: Two dimensional geoelectric structure along the profile. The epicenters of the 1956 Anjar earthquake given by Chandra 1977, and Chang and Gao (1997) are shown as stars. The seismic reflectors observed by Sarkar et al. (2007) are superimposed. Open circles represent the seismicity ($M_w \geq 3.0$) within 5km on either side of the profile. The Bouguer gravity anomaly (BGA) and topographic variations along the profile are shown in the top panels.

Figure 10: A plot showing variation of (a) P wave velocity (V_p) model and (b) density with depth beneath the three seismic stations shown in figure 1. The level of neutral buoyancy is taken from Glazner and William (1988)

Figure 11: A cartoon showing the plausible geological interpretation of the MT models in Kachchh region.

x-x-x

Figures

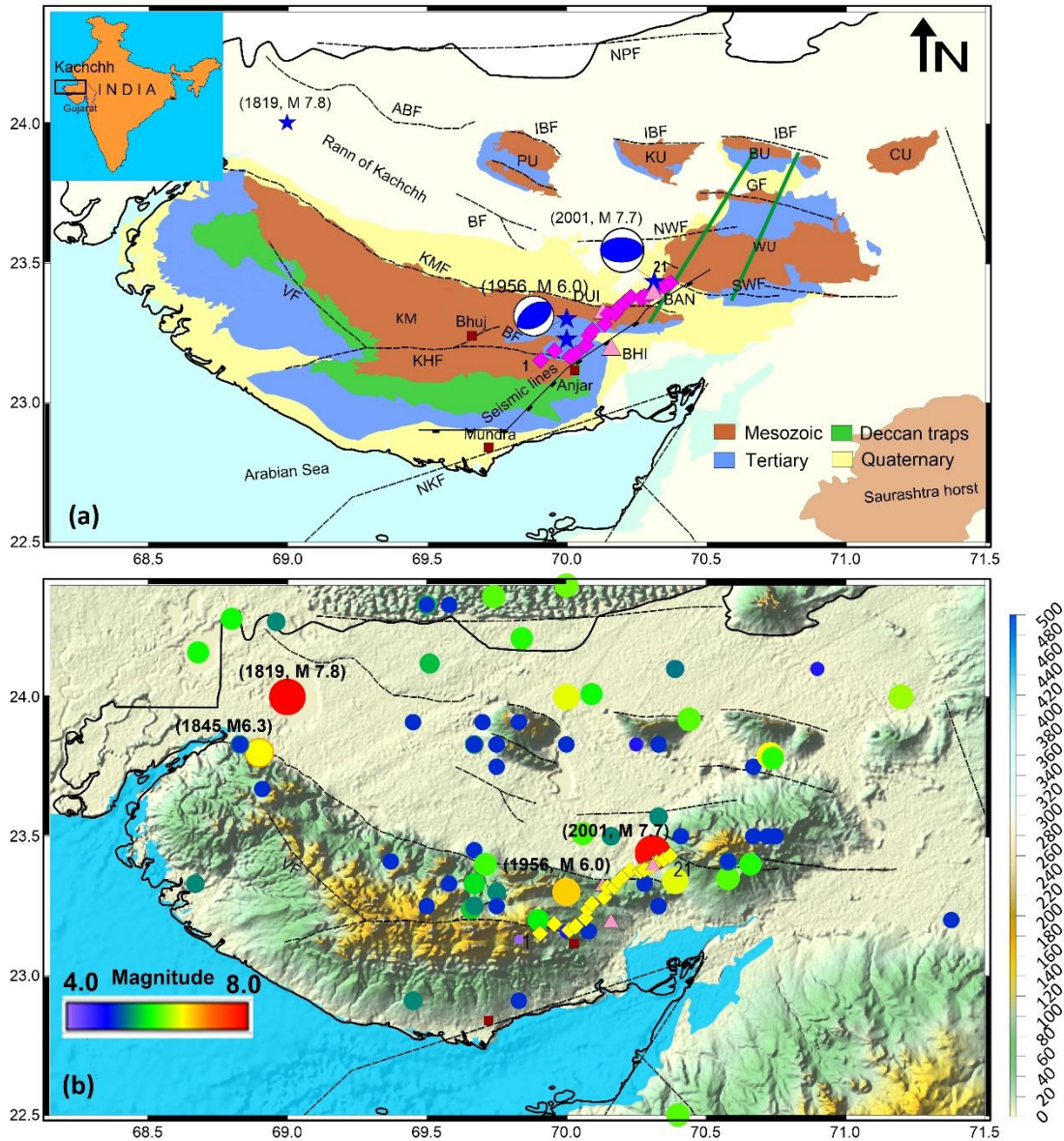


Figure 1a: Generalized geotectonic map of the Kachchh region showing the MT sites (magenta diamond symbols). Locations of the three significant earthquakes (Allahbund, Anjar and Bhuj earthquakes) are also shown along with the respective focal mechanisms. The seismic stations and the profile along which Deep Seismic Sounding data are acquired (Sarkar et al. 2007) are shown as triangles and solid line respectively. The solid green lines are the MT profiles of Pavan Kumar et al. (2017). Here, NPF :Nagar Parkar F. IBF: Island Belt F., ABF :Allahbund F. BF :Banni F., KMF : Kachchh Mainland F. Bh F :Bhuj F. , KHF : Katrol Hill F., NWF : Nagar Parkar F., SWF : South Wagad Fault, NKF : North Katiyawar Fault. Figure 1b: Topographic map of the Kachchh region showing locations of the past and historic earthquakes.

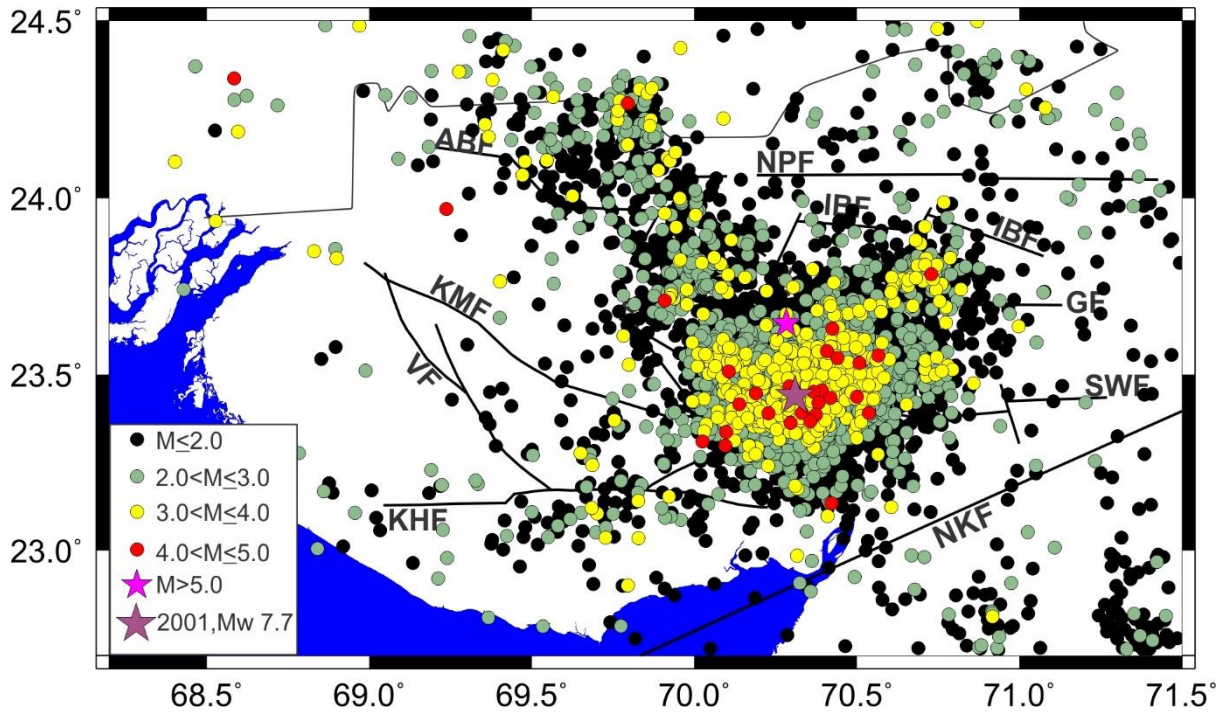


Figure 2: Seismicity of the Kachchh region during 2007-17 shown together with the 2001 Bhuj main shock.

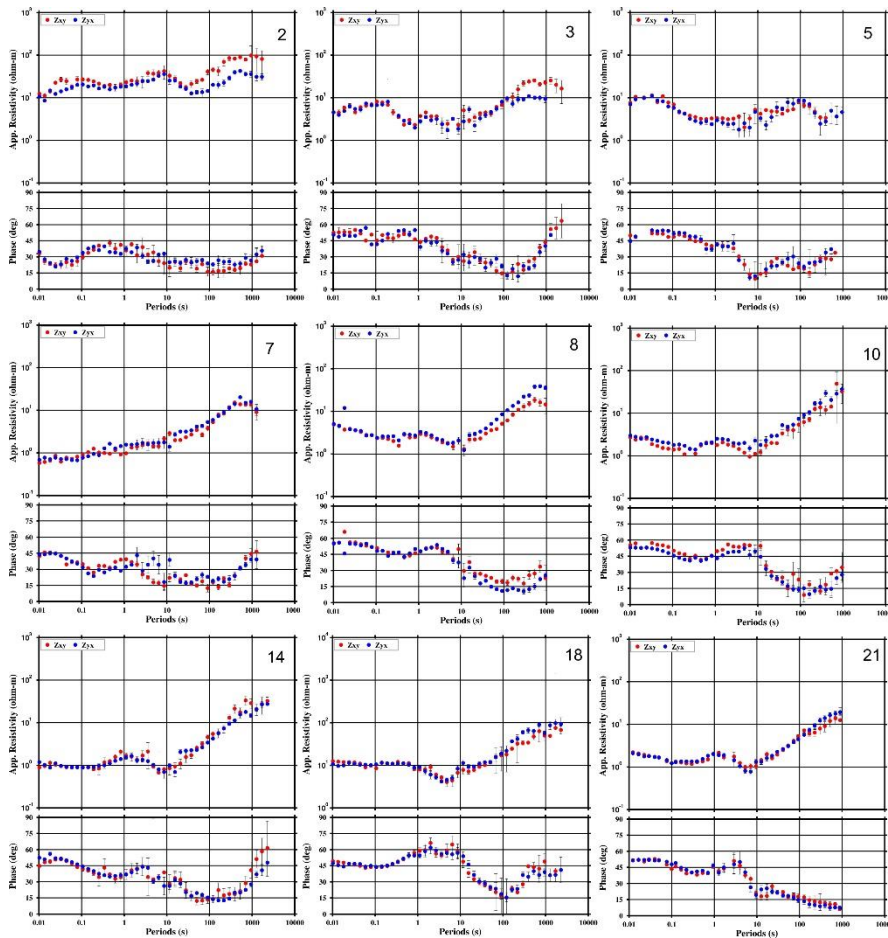


Figure 3: Apparent resistivity and phase curves for 9 sites along the profile.

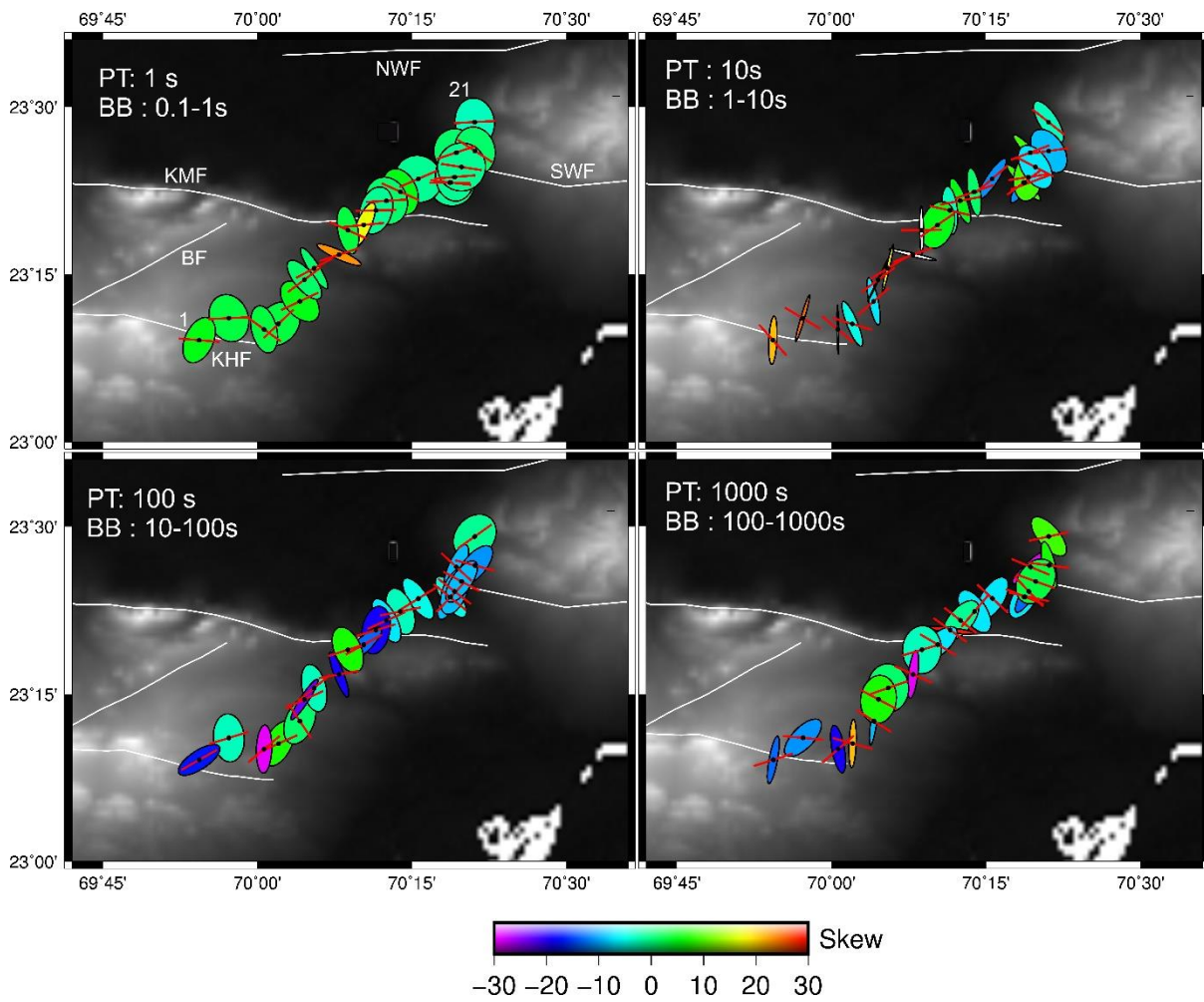


Figure 4: Phase ellipses (for 1s, 10s, 100s and 1000s) obtained from PT analysis and strike directions (bars) estimated from BB approach in the four period bands (0.1-1s, 1-10s, 10-100s and 100-1000s). The minor axes of the phase ellipses are normalized to their major axes to maintain an equal size for the ellipses.

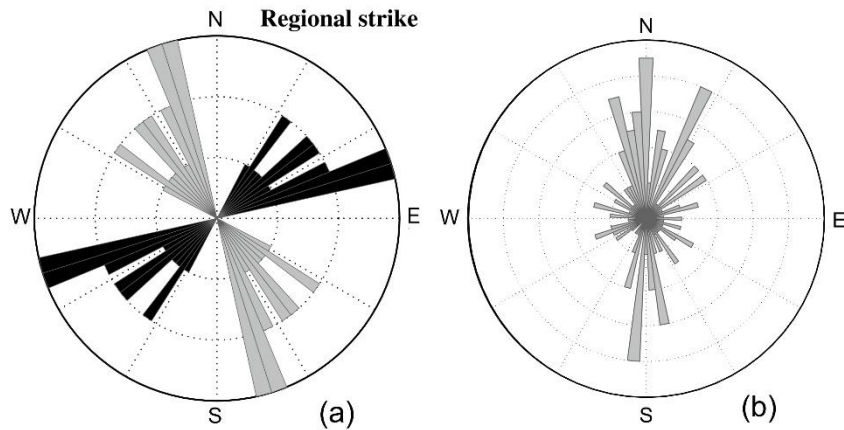


Figure 5: a) Rose diagram obtained after multi frequency single site analysis following the BB approach. The 90° ambiguity of the impedance tensor analysis results in the cross-shaped diagram b) Rose diagram for the induction vectors for the period band of 1-1000s

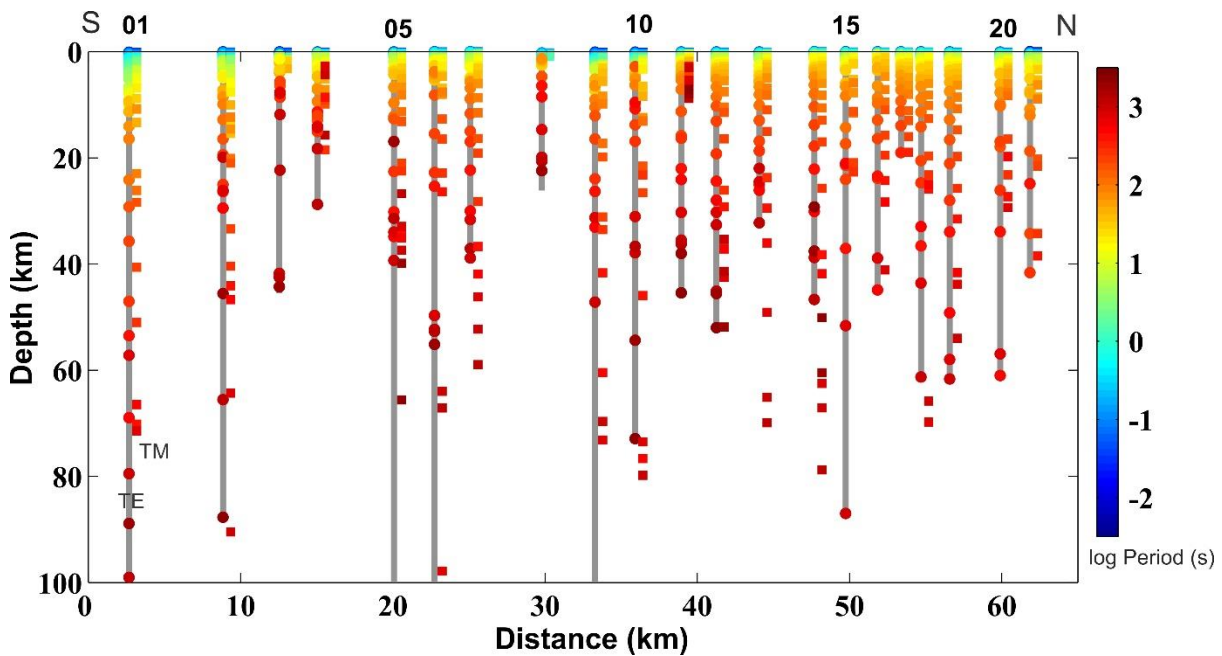


Figure 6: Niblett-Bostick penetration depths for all sites on the profile. The penetration depths are plotted separately for the TE and TM modes at each site.

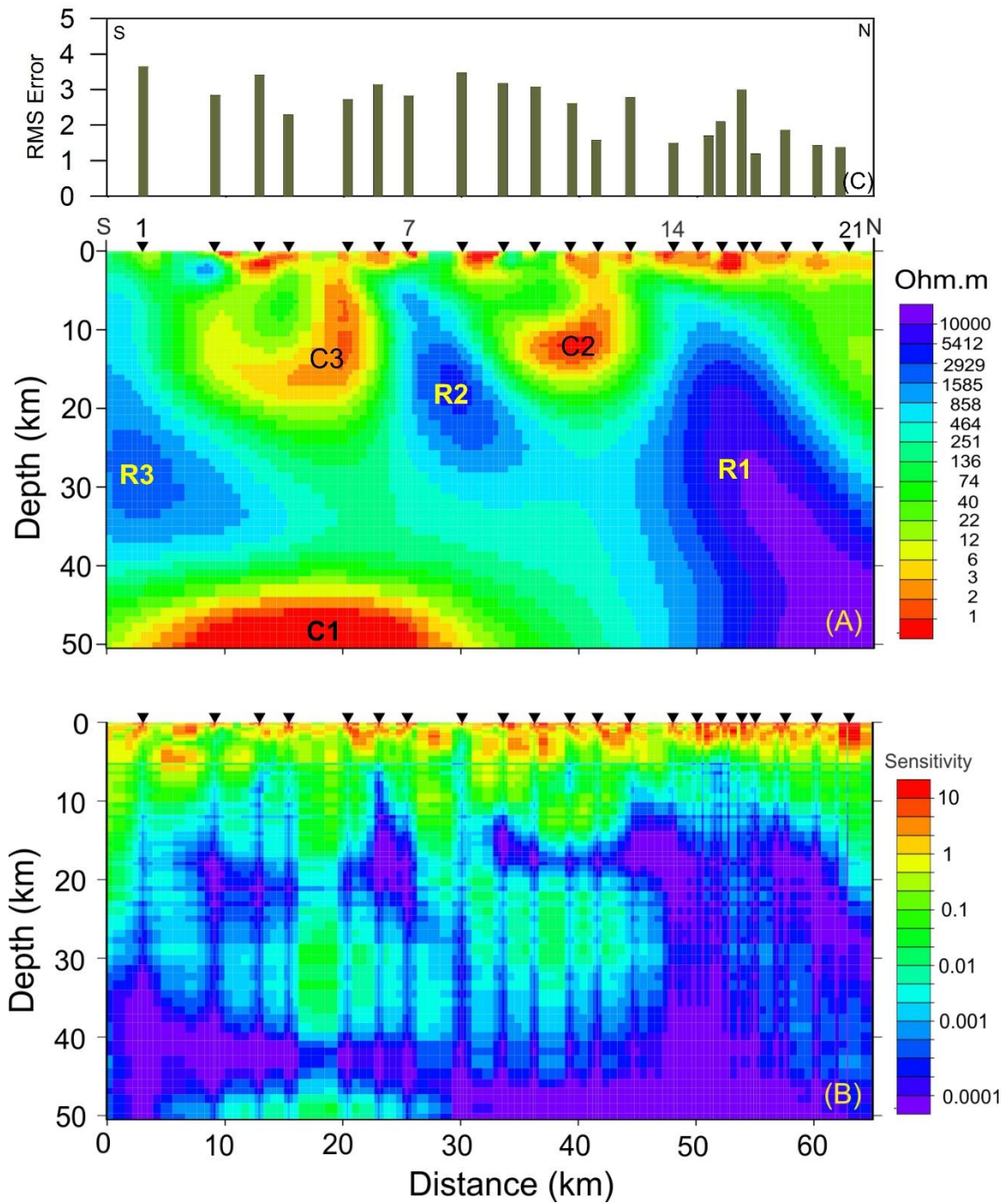


Figure 7: (a) 2-D geoelectric structure of the study region (b) corresponding sensitivity map; A large value of the sensitivity parameter (red, yellow, and green colors) indicates a well-resolved region and (c) RMS error shown site-wise

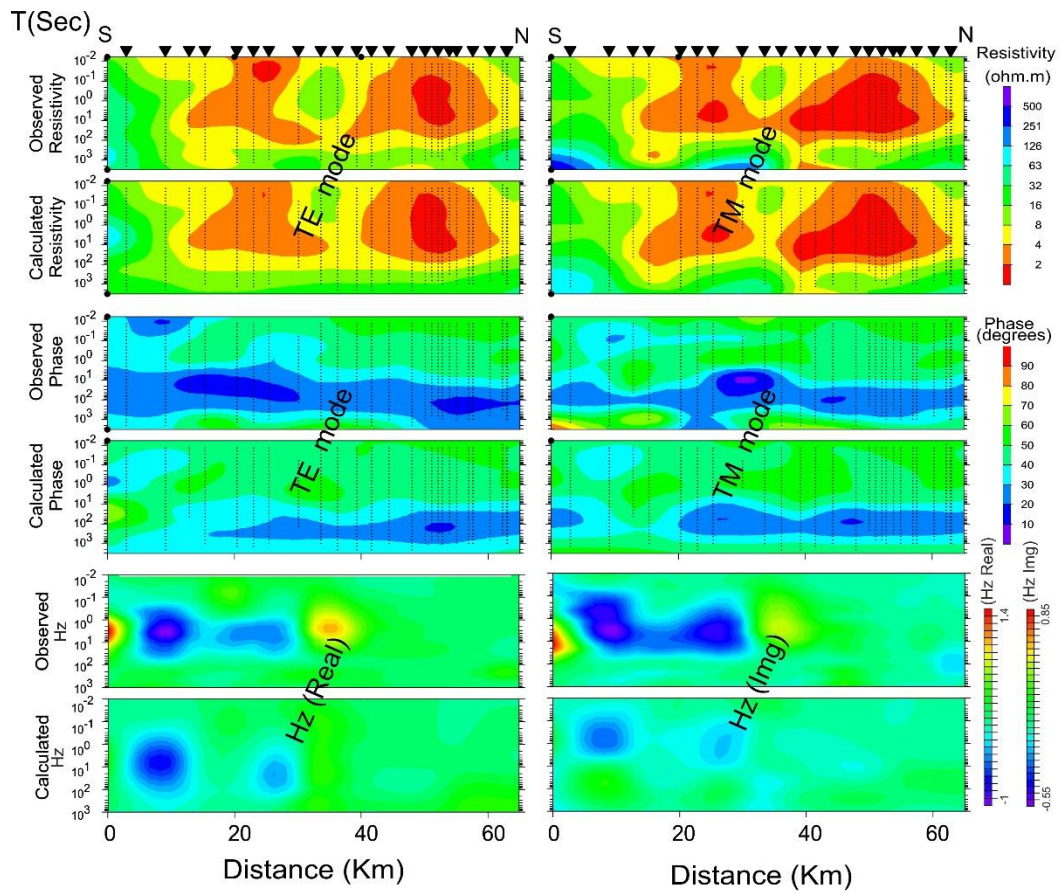


Figure 8: Pseudo sections showing fit between the observed and calculated MT data

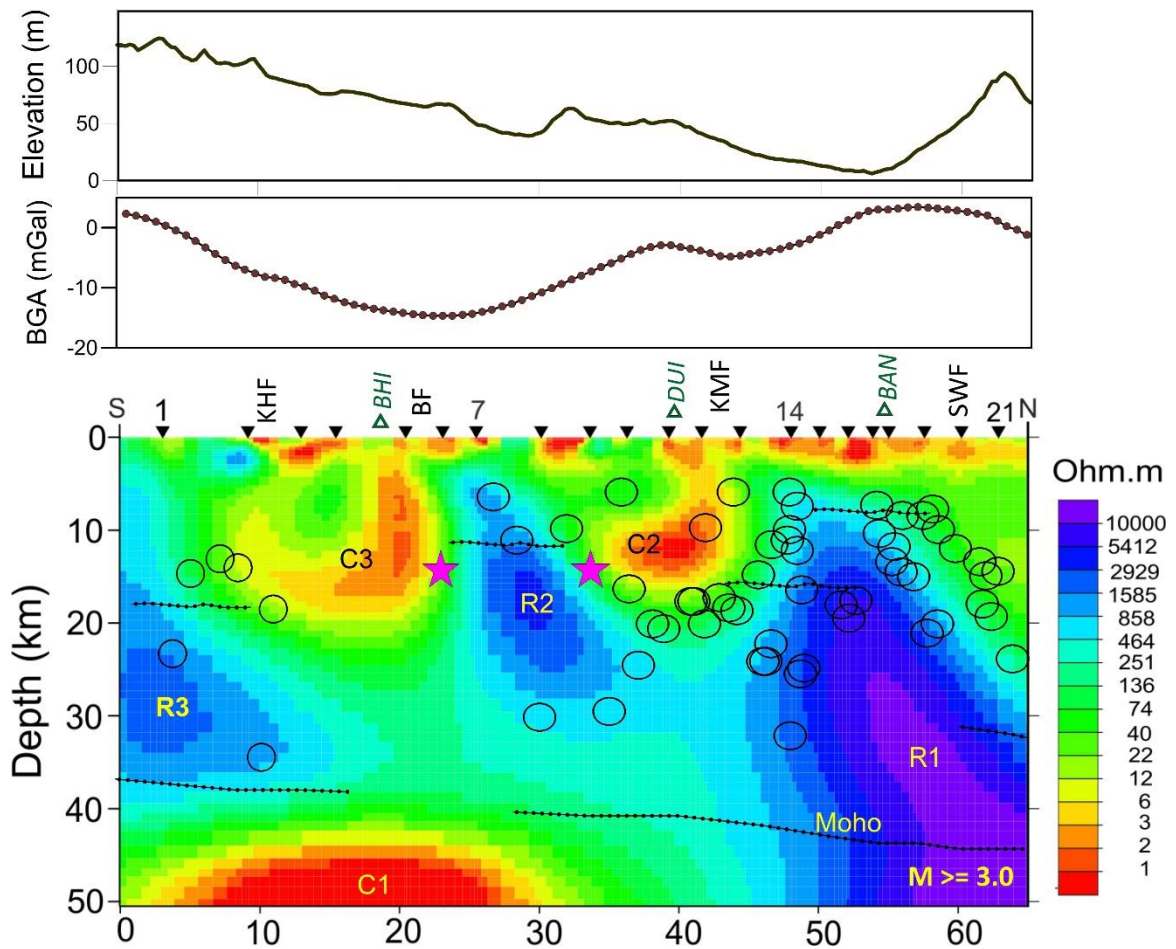


Figure 9: Two dimensional geoelectric structure along the profile. The epicenters of the 1956 Anjar earthquake given by Chandra 1977, and Chang and Gao (1997) are shown as stars. The seismic reflectors observed by Sarkar et al. (2007) are superimposed. Open circles represent the seismicity ($M_w \geq 3.0$) within 5km on either side of the profile. The Bouguer gravity anomaly (BGA) and topographic variations along the profile are shown in the top panels.

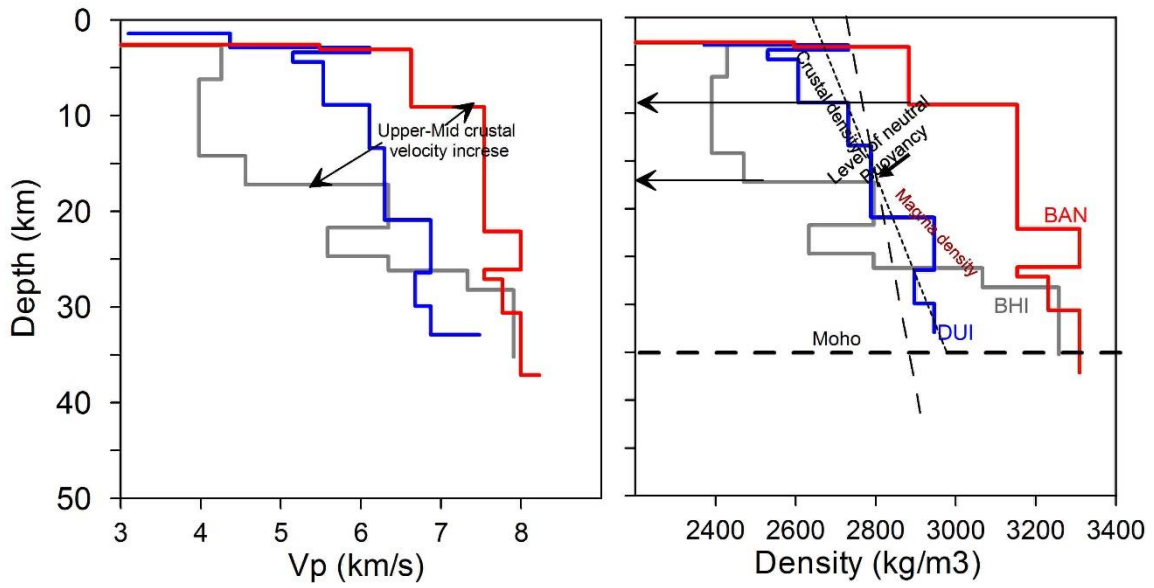


Figure 10: A plot showing variation of (a) P wave velocity (V_p) model and (b) density with depth beneath the three seismic stations shown in figure 1. The level of neutral buoyancy is taken from Glazner and William (1988)

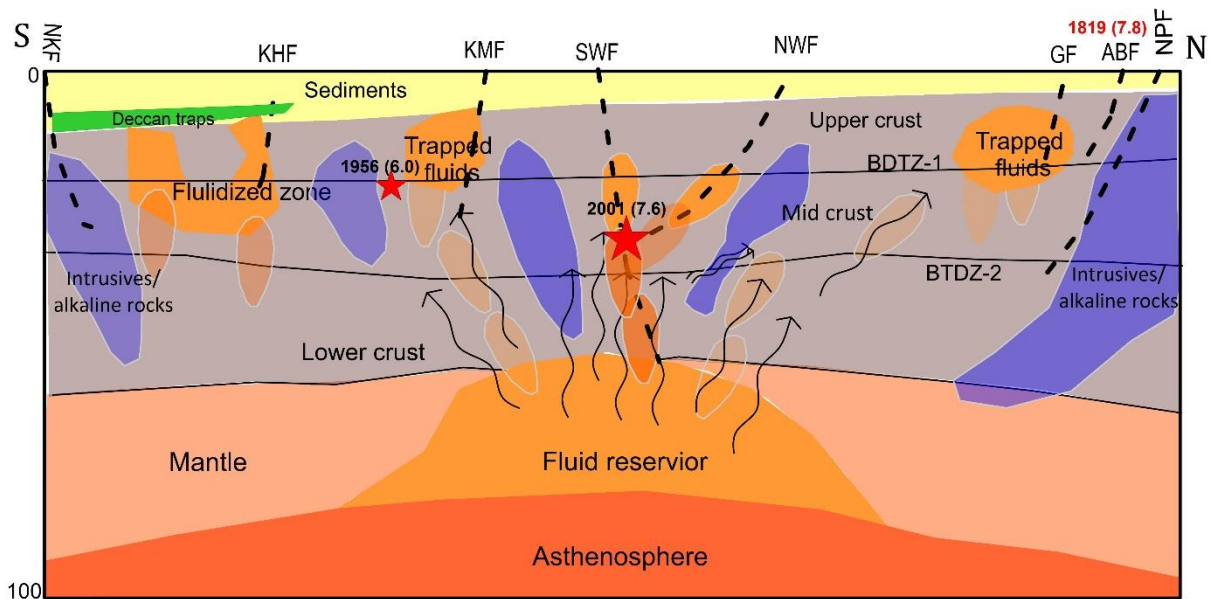


Figure 11: A cartoon showing the plausible geological interpretation of the MT models in Kachchh region.

Supplementary Information

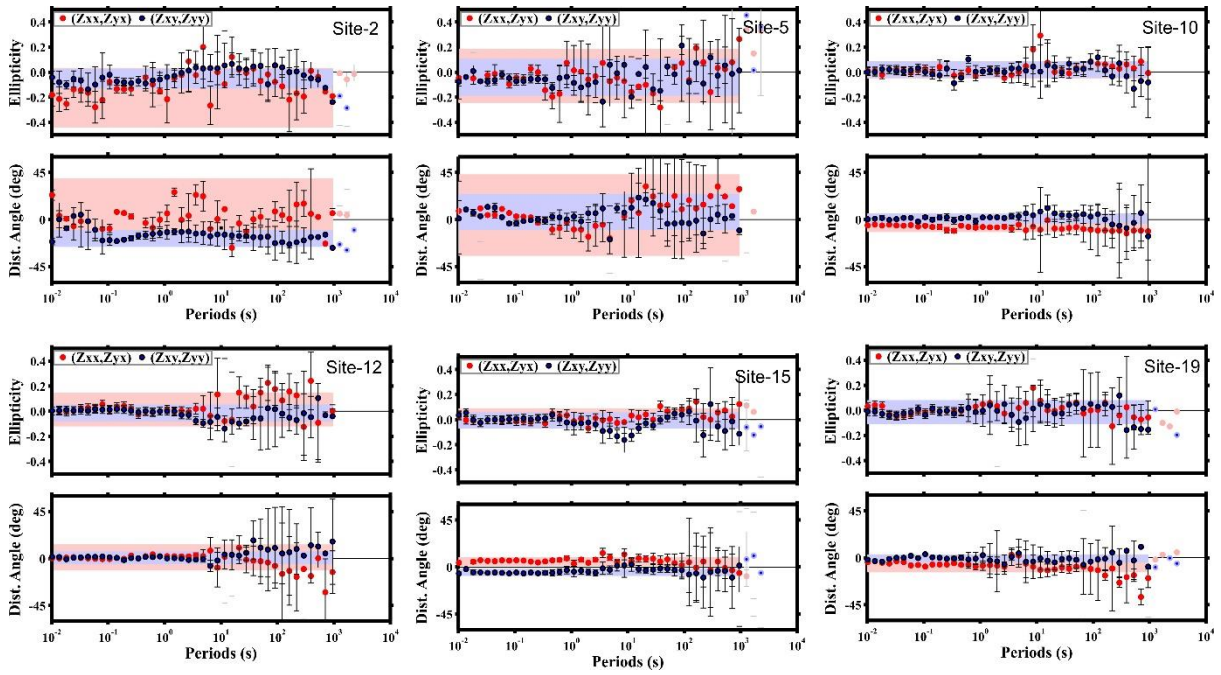


Figure S1: Distortion parameters after BB decomposition analysis for few sites

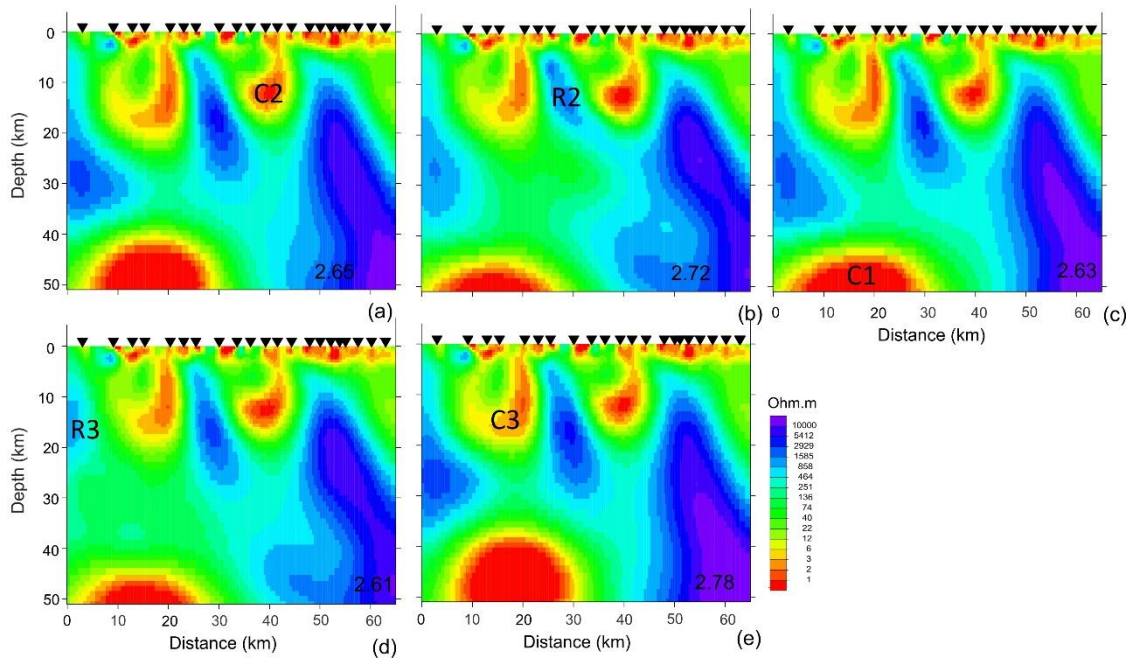


Figure S2 : Goelectric models after constrained inversion of various features- a) Conductor C2, b) Resistor, R2, c) Conductor, C1, d) Resistor, R3 and e) Conductor C3

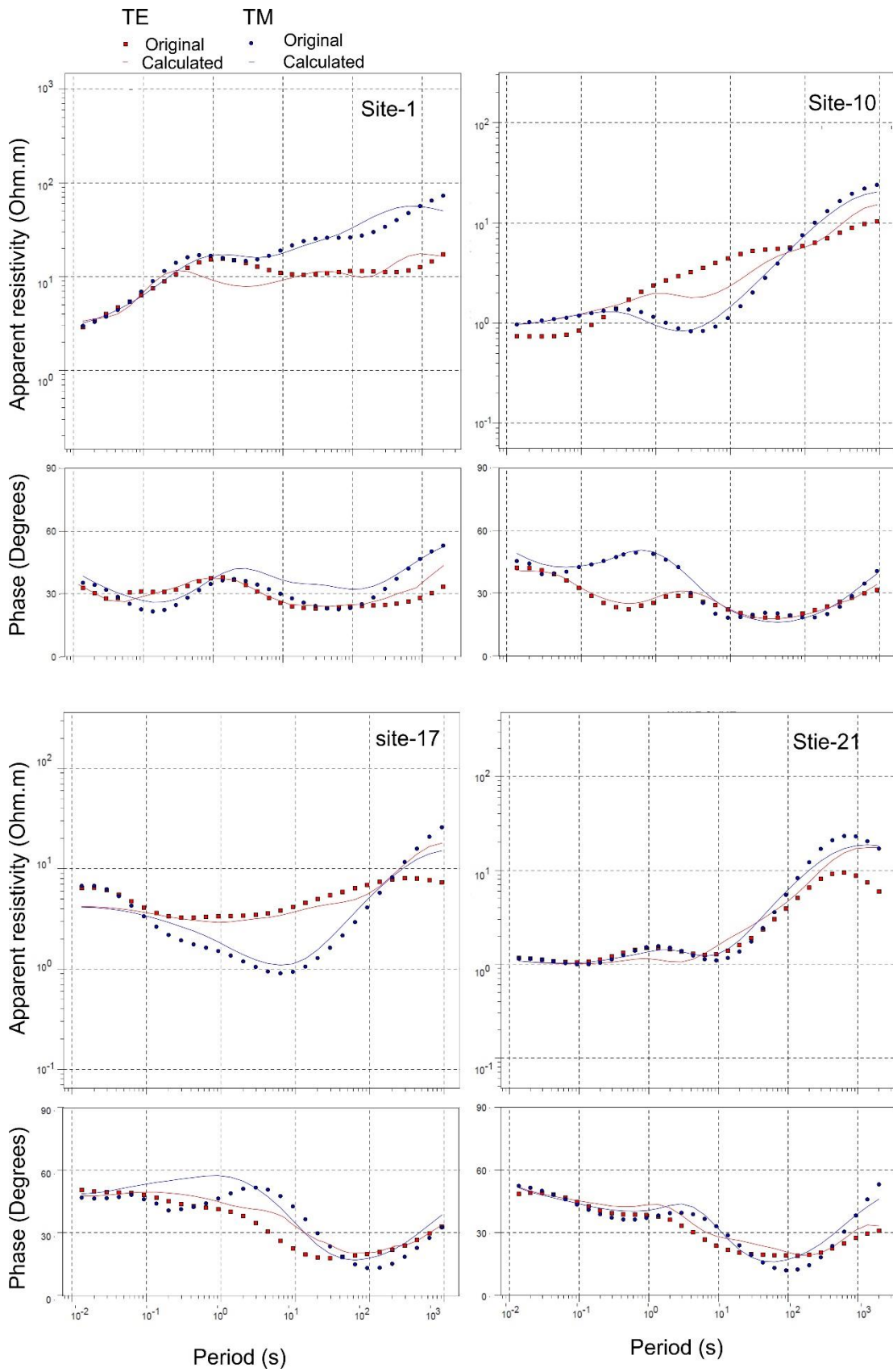


Figure S3 : Fit between observed and calculated apparent resistivity and phase curves for some sites along the profile.

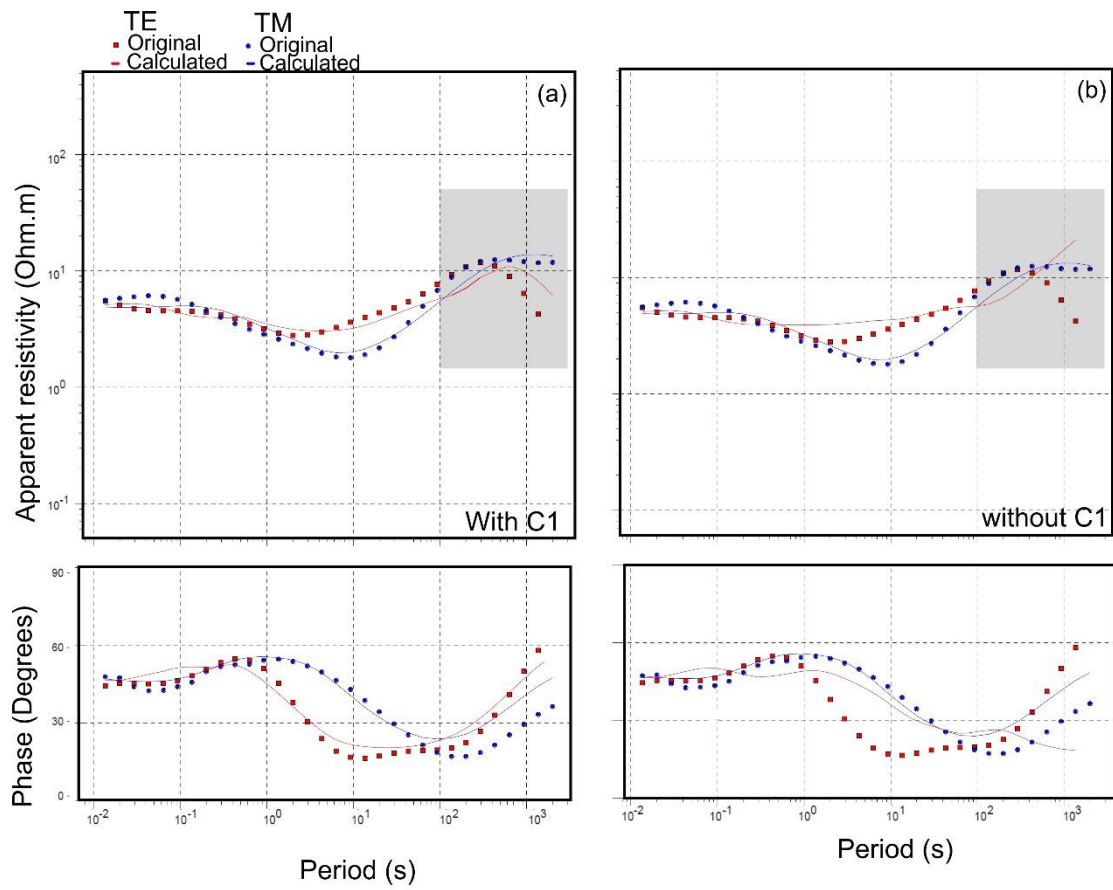


Figure S4: Forward modelling response (solid line) and observed responses (symbols) for a) with conductor C1 and b) without conductor C1